Studies on Synthesis and Properties of Mixed Oxides Containing Bivalent Europium and Niobium

(ユウロピウム(II)とニオブを含む複合酸化物の合成と物性に関する研究)

1983

KENJI ISHIKAWA

PREFACE

The work described in this thesis was carried out under the guidance of Professor Jiro Shiokawa of the Department of Applied Chemistry, Faculty of Engineering, Osaka University.

The object of this thesis is to describe preparation and properties of mixed oxides containing bivalent europium and niobium, and appreciate their possibilities for electrical materials. The author hopes that the work described in this thesis would give a suggestion on developing new electrical materials.

K. Ishikawa

Kenji Ishikawa

Suita, Osaka
January, 1983

CONTENTS

GENERAL INTRODUCTION

Since some systematic separation techniques have been established for a lanthanide series, lanthanide compounds of high purity become available as raw materials at moderate cost, and many investigations have been done for compounds containing rare earth elements. Recently, some lanthanide compounds have been used as functional materials such as magnets and phosphors. The objects of this study are to synthesize and to characterize mixed oxides containing europium and niobium in order to develop some useful materials.

Lanthanide ions are usually in the trivalent state, because lanthanides are IIIb group elements. Lanthanide ions can also exist in a bivalent state under limited conditions. For example, bivalent europium, ytterbium, and samarium ions have been identified in metals, crystals, and complexes [1-6]. The bivalent europium ion is the most stable and many europium (II) mixed oxides are reported to be found [7-19]. However, the reducing power of the bivalent europium is so strong that cations being able to coexist with it are limited [20,21].

Niobium is an element which can coexist with the bivalent europium cation in mixed oxides [20,21]. Niobium is also known to form bronze compounds with some bivalent ions ($A^{2+}_xNbO_3$) [22]. Bronze compounds have attracted much interest especially for their electrical properties, and stimulated various studies. However, there are few reports about mixed oxides of bivalent europium and niobium.

From the above point of view, preparation, structure, and

chemical and physical properties of the mixed oxides containing bivalent europium and niobium have been studied in the present work. The thesis is composed of three chapters and general conclusion.

In chapter 1, preparation, structure, and electrical properties of the europium (II) niobium bronze containing various europium and oxygen contents are described. A new compound, $Eu(II)_xNb(II)_{1-x}O$, which was found in the course of the study, is also mentioned in this chapter.

In chapter 2, oxidation of the europium (II) niobium bronzes is discussed in detail.

In chapter 3, electrical properties of sintered $EuZrO_3$ - $EuNbO_3$ and sintered $EuTiO_3$ - $EuNbO_3$ are described. The chapter is an application study of the bronzes for developing new electrical resistor materials whose thermal coefficient of electrical resistivity is very small.

The papers published by the author concerning the present studies are as follows:

1. Electrical properties of divalent europium niobium bronzes Eu_xNbO_3.
   K. Ishikawa, G. Adachi, M. Hasegawa, K. Sato, and J. Shiokawa,
   J. Electrochem. Soc., 128, 1374 (1981).
2. Preparation and oxidation of europium (II) niobium bronze Eu_xNbO_{3-y}.
   K. Ishikawa, G. Adachi, M. Tanida, and J. Shiokawa,

Bull. Chem. Soc. Jpn., 54, 159 (1981).

3. Electrical properties of sintered $EuZrO_3$ - $EuNbO_3$ and $EuNbO_3$.
K. Ishikawa, G. Adachi, and J. Shiokawa,
Mat. Res. Bull., 16, 419 (1981).

4. Preparation and electrical properties of $Eu(II)_xNb(II)_{1-x}O$.
K. Ishikawa, G. Adachi, and J. Shiokawa,
Chem. Lett., 1982, 623.

5. Preparation and electrical properties of $Eu(II)_xNb(IV)O_{2+x}$.
K. Ishikawa, G. Adachi, and J. Shiokawa,
Bull. Chem. Soc. Jpn., 55, 3317 (1982).

6. Electrical properties of sintered $EuTiO_3$ - $EuNbO_3$.
K. Ishikawa, G. Adachi, and J. Shiokawa,
Mat. Res. Bull., in press.

7. Europium niobium bronzes.
K. Ishikawa, G. Adachi, and J. Shiokawa,
Mat. Res. Bull., in contribution.

Chapter 1

PREPARATION, STRUCTURE, AND ELECTRICAL PROPERTIES OF EUROPIUM (II) NIOBIUM BRONZES

1-1. Introduction

Only a few metal oxide systems have metallic properties. Most of them are lower oxides of transition metals, e.g., ReO_3, NbO, and VO [23]. Some of the tungsten bronze type oxides, their general formula A_xBO_3, also exhibit metallic conduction [23,24]. Especially, a number of experimental and theoretical work have been done to describe the electrical properties of the cubic sodium tungsten bronze [25-26]. A strontium niobium bronze, which has been first prepared by Ridgley et al. [22], also has a cubic structure and has a metallic character [23].

Greedan et al. have proposed an important guideline for the preparation of Eu^{2+} compound [20], in which the desired europium (II) oxide phase should have an Sr^{2+} analog, since ionic radii of Eu^{2+} and Sr^{2+} are almost equal [37]. The europium niobium bronze, Eu_xNbO_3, has been first synthesized by Greedan et al. [20,21]. The niobium bronze is a tungsten bronze like compound, and the crystal structure and the lattice size

closely resemble that of Sr_xNbO_3 [38-31]. In Eu_xNbO_3, most of the europium ions are in the 2+ state and Nb^{4+} ions coexist with Nb^{5+} ions. Some of the europium ions are in a 3+ state, since the reducing power of niobium is not strong enough to reduce all Eu^{3+} to Eu^{2+} [42-45]. Greedan et al. [45], using Eu-151 Mössbauer spectroscopy, have confirmed that Eu^{3+} ions coexist with Eu^{2+} in Eu_xNbO_3 at low x.

For Eu_xNbO_3, ratios of Eu^{2+} to total Eu and Nb^{4+} to total Nb are determined only by x. The ratio of Nb^{4+} to total Nb should affect the electrical properties of Eu_xNbO_3, since the number of Nb^{4+} ions is equal to that of conduction electrons for the cubic bronze. However, the Nb^{4+} to total Nb ratio is also controlled by removing lattice oxygen from Eu_xNbO_3. The lattice oxygen can be removed untill all the Nb^{5+} ions are reduced to the Nb^{4+} ions, i.e., forming $Eu^{2+}_xNb^{4+}O_{2+x}$.

Electrical properties of Eu_xNbO_3 have been reported by Studer et al. [42-44], although their study has been limited to oxygen stoichiometric Eu_xNbO_3 of low x ($x = 0.5$ and 0.6).

In this chapter, the europium niobium bronze is expressed by Eu_xNbO_y, and the structure and the electrical properties of the bronze with various x and y are discussed.

1-2. Experimental

Reagents

Europium sesquioxide (Shin-etsu Chemical Corp., minimum purity 99.99%), diniobium pentoxide and niobium metal (Wako

Chemical Industries, Ltd., purity 99.99% and 99.9%, respectively). Europium sesquioxide and diniobium pentoxide were calcinated at 1000 K for half an hour in the air before being weighed.

Preparative

A fully mixed powder of Eu_2O_3, Nb_2O_5, and Nb was pressed into pellets. The pellets were packed into a Mo box and sealed in a silica tube under vacuum. The pellets were degassed under vacuum at 450 K for 3 h before the sealing procedure. The silica tube was set up in a vertical furnance and heated at 1423-1473 K for 6 h. The sample was ground in an agate mortar, re-pressed into pellets, degassed, sealed in a silica tube under vacuum and heated again at 1423-1473 K for 30-50 h. The reaction was completed during the procedure described above and assumed to proceed as follows.

$$0.5xEu_2O_3 + (0.2y-0.3x)Nb_2O_5 + (1+0.6x-0.4y)Nb \longrightarrow Eu_xNbO_y \quad (1)$$

However, in practice niobium metal was taken 1.05 times the amount needed to prepare Eu_xNbO_y to compensate for slight oxidation losses of the samples during the synthetic procedure.

Analyses

The phase purity and the structure type of Eu_xNbO_y were characterized by a x-ray powder diffraction method with a Rigaku Denki "Rotor-flex" diffractometer.

The atomic ratios, x in Eu_xNbO_y, were determined by a fluorescent x-ray analytical method with a Rigaku Denki energy dispersion type x-ray fluorescent spectrograph unit "Ultra trace system" having a tungsten target x-ray tube, a stannum second

target, and a Si(Li) semiconductor detector.

The oxygen contents, y in Eu_xNbO_y, were analysed by a thermal gravimetric analysis. The niobium bronze was fired in a platinum crucible at 1100 K. From the weight gain due to oxidation and europium content (x), the oxygen content (y) was determined. The y value was given by regarding the oxidation reaction as follows:

$$Eu_xNbO_y + (0.75x-0.5y+1.25)O_2 \longrightarrow 0.5xEu_2O_3 + 0.5Nb_2O_5 \qquad (2)$$

Magnetic Measurements

Magnetic susceptibility measurements were done for Eu_xNbO_y with a Shimadzu magnetic balance "MB-11" at 4.2-300 K.

Electrical Resistivity Measurements

The electrical resistivity measurements for the sintered samples were carried out in a helium atmosphere from 4.2 to 373 K. A simple four-probe d.c. method was employed for the resistivity measurements of the samples. Rectangular samples of about 2 mm^2 in cross section and 8-12 mm long were taken for the measurements with the four-probe method. The samples were cut from the sintered pellets of 13 mm in diameter and 1 mm in thickness, and the surfaces of the samples were finished with No. 1000 carborundum paper. Electrical leads were attached to the faces of each sample with Ag paste. The resistivity measurements were performed in the potential region in which the samples behaved ohmically. Furthermore, to avoid any contributions to the measured potential from thermally generated emf's readings were taken in both forward and reverse directions and

the averaged values were recorded.

Thermoelectric Power Measurements

Thermoelectric power measurements were carried out in a helium atmosphere from 100 to 373 K. A rectangular sample of about 2 mm^2 in cross section and about 4 mm long was attached to two copper blocks with Ag paste. A thermal gradient was produced across the sample by small heaters attached to the copper blocks, and the temperature difference across the sample was regulated so as to fall within 10 K. The Seebeck coefficient of the sample was determined according to the relation:

$$S = S_{Cu} - \Delta V/\Delta T, \qquad (3)$$

where S_{Cu} is the absolute Seebeck coefficient of copper [46], ΔV is the thermoelectric voltage of the sample, and ΔT is the temperature difference across the sample.

1-3. Results and Discussion

a. Eu_xNbO_3 and Eu_xNbO_{2+x}

Crystal Structure

The phases and analytical data for Eu_xNbO_3 and Eu_xNbO_{2+x} obtained are listed in Table 1. Niobium bronze Eu_xNbO_3 of $x = 0.5$-0.65 has a tetragonal form [38,47] and for $x = 0.65$-1.0 has a cubic form [38,47], while Eu_xNbO_{2+x} has a cubic form in the single phase region ($x = 0.5$-1.0).

Lattice constants of cubic Eu_xNbO_3 and Eu_xNbO_{2+x} are plotted in Fig. 1 as a function of the europium concentration x.

Table 1. Analytical and crystal data for Eu_xNbO_3 and Eu_xNbO_{2+x}

Exptl No.	Eu_xNbO_y (nominal)		Eu_xNbO_y (analytical)		Phase	a(cubic)	a(tetragonal)	c(tetragonal)
	x	y	x	y		Å	Å	Å
Eu_xNbO_3								
A	1.00	3.00	1.01	3.01	Cubic	4.026		
B	0.90	3.00	0.90	3.00	Cubic	4.010		
C	0.85	3.00	0.88	3.03	Cubic	4.009		
D	0.80	3.00	0.82	3.03	Cubic	4.002		
E	0.75	3.00	0.76	3.03	Cubic	3.985		
F	0.70	3.00	0.70	3.09	Cubic	3.980		
G	0.65	3.00	0.68	3.05	Cubic	3.978		
H	0.60	3.00	0.60	3.03	Tetragonal	—	12.361	3.885
I	0.55	3.00	0.58	3.02	Tetragonal	—	12.363	3.892
J	0.50	3.00	0.51	3.02	Tetragonal	—	12.355	3.901
Eu_xNbO_{2+x}								
A	1.00	3.00	1.01	3.01	Cubic	4.026		
K	0.90	2.90	0.90	2.94	Cubic	4.013		
L	0.80	2.80	0.79	2.93	Cubic	3.993		
M	0.70	2.70	0.71	2.82	Cubic	3.992		
N	0.60	2.60	0.62	2.70	Cubic	3.983		
O	0.50	2.50	0.52	2.66	Cubic	3.977		
P	0.50	2.50	0.51	2.47	Cubic+u[a)]	3.988		
Q	0.45	2.45	0.47	2.38	Cubic+u	3.990		
R	0.40	2.40	0.42	2.39	Cubic+u	3.982		
S	0.30	2.30	0.30	2.16	Cubic+u	3.982		

a) u: Unknown phase.

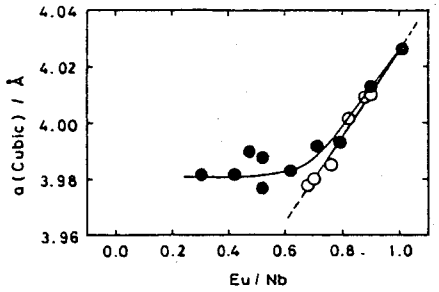

Fig. 1. Lattice constants vs. Eu concentration for Eu_xNbO_3 (O) and Eu_xNbO_{2+x} (●)

The cubic lattice constant of Eu_xNbO_3 increases almost linearly with an increase in x [47]. The least-squares fitting generates the following equation:

$$a(\text{cubic}) = 3.974 + 0.1515x \quad (\text{Å}) \qquad (4)$$

Lattice constants of Eu_xNbO_{2+x} also increase with increase in x in the range from x = 0.5 to x = 1.0, but the change is not linear and the constants of Eu_xNbO_{2+x} are greater than those of Eu_xNbO_3 on a fixed composition especially below x = 0.7. Below x = 0.5, an unknown phase appeared in addition to a cubic phase of a = 3.982 Å, and the tetragonal phase which was found in Eu_xNbO_3 of x = 0.5-0.65 was not observed.

The phase change of Eu_xNbO_3 from a cubic to a tetragonal form is explained as follows. The crystal structure of the cubic and the tetragonal niobates are revealed in Fig. 2 (a) and (b). A bivalent europium cation occupies a body-centered site of the cubic lattice (Fig. 2 (a)) and the site expressed by the black circle in the tetragonal cell (Fig. 2 (b)). Since

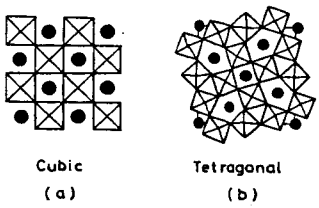

Fig. 2. Schematic diagram for the cubic and the tetragonal Eu_xNbO_3. The bivalent europium cation can occupy the position expressed by the black circles

the lattice constant decreases with a decrease in the europium concentration for cubic Eu_xNbO_3, the maximum ionic radius to be able to occupy the body-centered site of the perovskite structure also decrease with decreasing the europium concentration, and at x = 0.65 the maximum ionic radius becomes equal to the ionic radius of Eu^{2+}. At x = 0.65, the lattice constant "a" is 3.987 $\pm$ 3 Å and the tolerance factor "r" [48] is 1.01. The tolerance factor is defined by the following equation:

$$t = (r(Eu^{2+}) + r(O^{2-}))/\sqrt{2}a, \qquad (5)$$

where $r(Eu^{2+})$ (1.45 Å: 6th coordination) and $r(O^{2-})$ (1.40 Å: 6th coordination) are ionic radii [37] of Eu^{2+} and O^{2-} and a (3.987 Å for $Eu_{0.67}NbO_3$) is a cubic lattice constant. Below x = 0.65, the body-centered site of cubic Eu_xNbO_3 can no longer accomodate a bivalent europium cation and the cubic phase transform to the tetragonal phase. This can provide room for a bivalent europium cation in the limited range from x = 0.5 to

$x = 0.65$.

The above discussion is also applicable to Eu_xNbO_{2+x}. The lower limit of the lattice constant for cubic Eu_xNbO_{2+x} seems to be almost the same as the lattice size of $Eu_{0.65}NbO_3$. However, the tetragonal phase, which was found for Eu_xNbO_3 at $x = 0.5$-0.65, was not found and an unknown phase was detected in Eu_xNbO_{2+x} below $x = 0.5$.

Magnetic Properties

Results of the magnetic susceptibility measurements for Eu_xNbO_y are listed in Table 2. The observed magnetic moments are compared with the theoretical values, which are calculated in two ways. One of the theoretical moments is obtained by assuming that the 4d spins of niobium are unpaired, and the other is given by assuming that the spins are paired in the bronzes.

The observed magnetic moment of Eu_xNbO_3 is apparently smaller than either of the theoretical ones. The Eu^{3+} ions in Eu_xNbO_3 should exist, because niobium metal is not strong enough to reduce all Eu^{3+} to Eu^{2+}.

The observed magnetic moment for each Eu_xNbO_{2+x} fits well with the latter of the two theoretical moments. The finding that the bronze is a metallic 4d electron-conductor suggests that the 4d spins of niobium are paired. In Eu_xNbO_{2+x}, most of the europium ions are in the 2+ state.

Electrical Properties

Results of the resistivity measurements are shown in Figs. 3, 4, and 5. The resistivities are found to decrease with reciprocal temperature for Eu_xNbO_3 of low eurpium

Table 2. Magnetic and electrical data for Eu_xNbO_3 and Eu_xNbO_{2+x}

Exptl No.	Eu_xNbO_y (analytical) x	y	Magnetic moments μ_{eff}/μ_B (Obsd)	μ_{eff} [a] μ_B (Calcd)	μ_{eff} [b] μ_B (Calcd)	Conduction	S [c] $\mu V K^{-1}$	S_0 [d] $\mu V K^{-1}$	m^*/m_0 [e]
Eu_xNbO_3									
A	1.01	3.01	7.92	8.16	7.98	m[f]	−7.0	−3.26	2.1
B	0.90	3.00	7.61	7.68	7.52	m	−6.2	−3.77	1.6
C	0.88	3.03	7.36	7.58	7.45	m	−8.2	−4.10	2.0
D	0.82	3.03	7.16	7.31	7.19	m	−11.1	−4.63	2.4
E	0.76	3.03	6.80	7.03	6.92	m	−14.7	−5.36	2.7
F	0.70	3.09	6.34	6.69	6.64	m	−17.2	−8.74	2.0
G	0.68	3.05	6.46	6.61	6.54	m	−22.2	−7.81	2.8
H	0.60	3.03	6.04	6.18	6.15	s[g]	−182	—	—
I	0.58	3.02	5.89	6.07	6.05	s	−152	—	—
J	0.51	3.02	5.47	5.67	5.67	s	—	—	—
Eu_xNbO_{2+x}									
A	1.01	3.01	7.92	8.16	7.98	m	−7.0	−3.26	2.1
K	0.90	2.94	7.70	7.71	7.53	m	−6.2	−3.42	1.8
L	0.79	2.93	7.15	7.21	7.06	m	−8.3	−3.99	2.1
M	0.71	2.82	6.69	6.87	6.70	m	−12.9	−3.77	3.4
N	0.62	2.70	6.29	6.47	6.27	m	−12.8	−3.56	3.6
O	0.52	2.66	5.70	5.89	5.70	m	−18.8	−3.99	4.7
P	0.51	2.47	5.74	5.94	5.66	—	—	—	—
Q	0.47	2.38	5.50	5.73	5.41	—	—	—	—
R	0.42	2.39	5.22	5.47	5.18	—	—	—	—
S	0.30	2.16	4.36	4.77	4.35	—	—	—	—

a) μ_{eff} (calcd) $=\sqrt{x\mu^2(Eu^{2+})+(Nb^{4+}/Nb)\mu^2(Nb^{4+})}$; $\mu(Eu^{2+})=7.94\mu_B$; $\mu(Nb^{4+})=1.73\ \mu_B$. b) μ_{eff} (calcd) $=\sqrt{x}\mu(Eu^{2+})$. c) S: Observed absolute Seebeck coefficient at 300 K. d) S_0: Calculated absolute Seebeck coefficient at 300 K. e) m^*: Effective mass of electron; m_0: rest mass of electron. f) m: Metallic. g) s: Semiconductive.

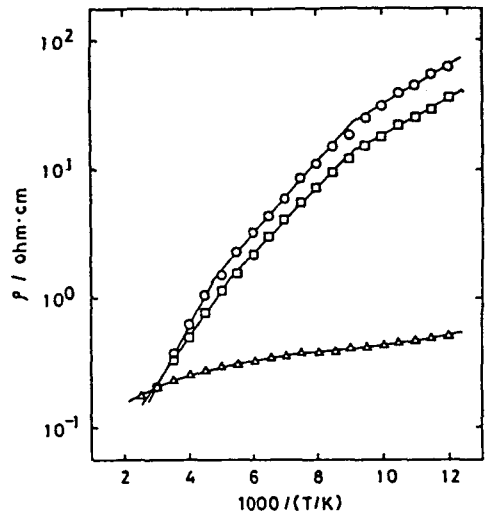

Fig. 3. Specific resistivities of the oxygen stoichiometric niobium bronze (tetragonal)

○ , $Eu_{0.60}NbO_{3.03}$
□ , $Eu_{0.58}NbO_{3.02}$
△ , $Eu_{0.51}NbO_{3.02}$

concentration (x = 0.5-0.65) (Fig. 3), and the changes are expressed by the well-known equation:

$$\rho = \rho_o \exp(E_a/kT), \qquad (6)$$

where Ea is related to the activation energy for conduction. The activation energy of $Eu_{0.51}NbO_{3.02}$, $Eu_{0.58}NbO_{3.02}$, and $Eu_{0.60}NbO_{3.03}$ is respectively 0.099, 0.084, and 0.033 eV at 300 K. Thermoelectric power measurements reveal that the samples

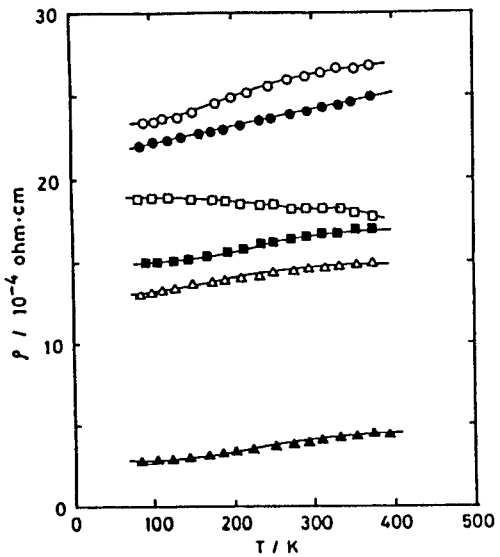

Fig. 4. Specific resistivities of the oxygen stoichiometric niobium bronze (cubic)

○ , $Eu_{0.90}NbO_{3.10}$
● , $Eu_{0.70}NbO_{3.09}$
□ , $Eu_{0.68}NbO_{3.05}$
■ , $Eu_{0.82}NbO_{3.03}$
△ , $Eu_{0.88}NbO_{3.03}$
▲ , $Eu_{0.76}NbO_{3.03}$

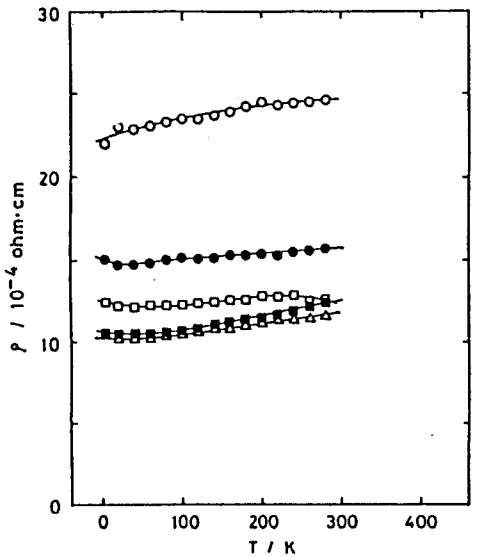

Fig. 5. Spicific resistivities of the niobium bronze having full oxygen vacancies (cubic)

○ , $Eu_{0.71}NbO_{2.82}$
● , $Eu_{0.62}NbO_{2.70}$
□ , $Eu_{0.52}NbO_{2.66}$
■ , $Eu_{0.90}NbO_{2.94}$
△ , $Eu_{0.79}NbO_{2.93}$

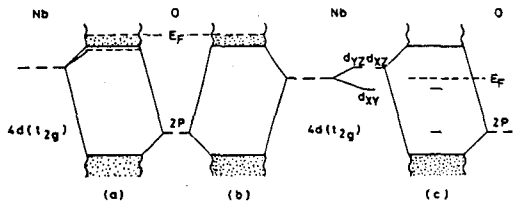

Fig. 6. Energy-level diagram for Eu_xNbO_{2+x} (a: cubic) and Eu_xNbO_3 (b: cubic; c: tetragonal)

are n-type semiconductors. However, the resistivities are found to decrease on decreasing the temperature for Eu_xNbO_3 of high europium concentration (x = 0.65-1.00) and Eu_xNbO_{2+x} (x = 0.5-1.0). In other words, the tetragonal samples are n-type semiconductors and the cubic samples are metallic conductors.

An interpretation of the electrical resistivity data for the tetragomal and cubic samples is given on the basis of Goodenough's model [23] for the tungsten bronze. The schematic band models for Eu_xNbO_3 and Eu_xNbO_{2+x} are illustrated in Fig. 6. The conduction bands of Eu_xNbO_y are formed by the 4d orbitals of niobium and the 2p orbitals of oxygen. All the $4d(t_{2g})$ orbitals of niobium are considered to be degenerated for cubic Eu_xNbO_3 (Fig. 6 (b)), and the number of conduction electrons is the same as the number of Nb^{4+} in this case. The number of Nb^{4+} in the general formula Eu_xNbO_y can be provided by the relation:

$$n = 2(x-y) + 5. \qquad (7)$$

The equation suggests that some conduction electrons exist

in the conduction band of cubic Eu_xNbO_3 (x = 0.65-1.0), giving all the cubic samples metallic properties. On the other hand, the $4d(t_{2g})$ orbitals of niobium in the tetragonal phase split into two states (Fig. 6(c)) and a localized nonbonding level ($4d_{xy}$) is formed below the bottom of the conduction band. The conduction electrons are considered to be trapped by the level, and the tetragonal bronzes exhibit semiconducting properties. From the analysis of the resistivity curve, the level is determined to be 0.1 eV below the bottom of the conduction band.

An energy level diagram for cubic Eu_xNbO_{2+x} is proposed in Fig. 6 (a). The conduction band is also composed of $4d(t_{2g})$ orbitals of niobium and 2p orbitals of oxygen. The $4d(t_{2g})$ levels of niobium, which are composed of $4d(t_{2g})$ orbitals around oxygen vacancies, are located below the conduction band.

The number of conduction electrons is equal to the number of Nb^{4+} as for Eu_xNbO_3, there is a Nb^{4+} per one formula of Eu_xNbO_{2+x}. Therefore, Eu_xNbO_{2+x} exhibits a metallic conduction (Fig. 5) as cubic Eu_xNbO_3 (Fig. 4). However the mobility of an electron and an effective mass of electron for Eu_xNbO_{2+x} should be different from those for Eu_xNbO_3, since positive charged oxygen vacancies are considered to attract the conduction electrons around the vacancies electrostatically.

In Figure 7, a.c. resistivities of some bronzes are plotted as a function of frequency. The a.c. resistivity of the tetragonal bronze decreases with increasing the frequency of alternating current more than 1000 kH_z. The grain-boundary effect may be responsible to the frequency dependence for the tetragonal bronze at high frequencies. However, the a.c.

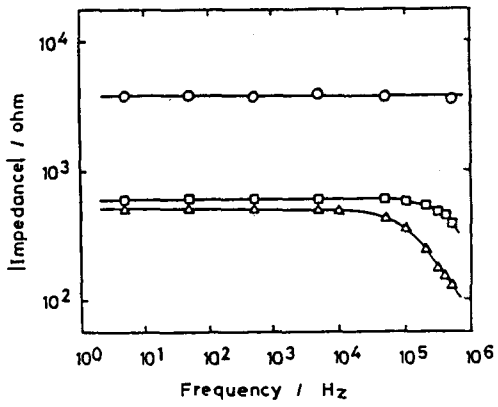

Fig. 7. A.c. resistivity of Eu_xNbO_3

□ , $Eu_{0.58}NbO_{3.02}$ (tetragonal)

△ , $Eu_{0.60}NbO_{3.03}$ (tetragonal)

○ , $Eu_{0.68}NbO_{3.05}$ (cubic)

resistivity of the cubic bronze is independent of the frequency of alternating current and there is no difference in results between by the d.c. and the a.c. methods.

Cubic Eu_xNbO_{2+x} has the same crystal structure and the same electrical conduction as cubic Eu_xNbO_3. However, an effective mass of electron for Eu_xNbO_{2+x} should be different from that for Eu_xNbO_3, since there are many oxygen vacancies in Eu_xNbO_{2+x}.

The Seebeck coefficients of cubic Eu_xNbO_3 and Eu_xNbO_{2+x} are given as a function of the temperature in Figs. 8 and 9. For the free-electron approximation [49] the Seebeck coefficient is given by the relation:

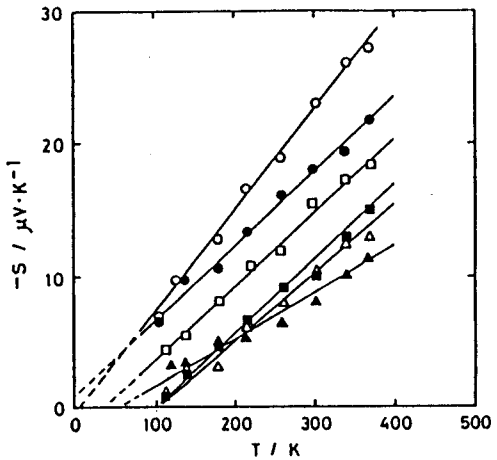

Fig. 8. Temperature dependence of the Seebeck coefficient for Eu_xNbO_3 (cubic)

○ , $Eu_{0.68}NbO_{3.05}$
● , $Eu_{0.70}NbO_{3.09}$
□ , $Eu_{0.76}NbO_{3.03}$
■ , $Eu_{0.82}NbO_{3.03}$
△ , $Eu_{0.90}NbO_{3.10}$
▲ , $Eu_{0.88}NbO_{3.03}$

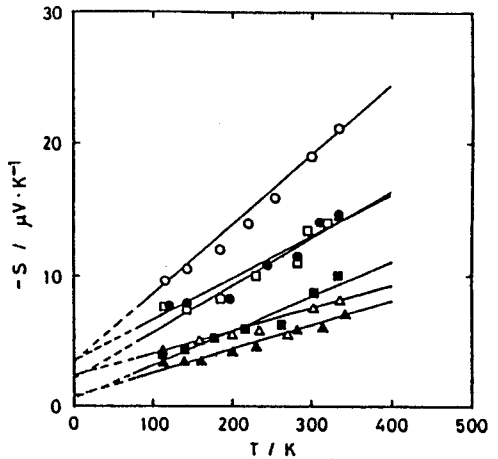

Fig. 9. Temperature dependence of the Seebeck coefficient for Eu_xNbO_{2+x} (cubic)

○ , $Eu_{0.52}NbO_{2.66}$
● , $Eu_{0.62}NbO_{2.70}$
□ , $Eu_{0.71}NbO_{2.82}$
■ , $Eu_{0.79}NbO_{2.93}$
△ , $Eu_{1.01}NbO_{3.01}$
▲ , $Eu_{0.90}NbO_{2.94}$

$$S = \frac{2}{3}\left(\frac{\pi}{3}\right)^{2/3} \frac{m^* k^2 T}{e(h/2\pi)^2} N^{-2/3}. \qquad (8)$$

An almost linear dependence of the Seebeck coefficient with temperature (Fig. 8) suggests that the conduction electrons are close to free electrons. The Seebeck coefficient of cubic Eu_xNbO_3 at 300 K are plotted in Fig. 10 as a function of the carrier concentration given by Eq. 9:

$$N = \frac{dL}{M}[2(x-y) + 5], \qquad (9)$$

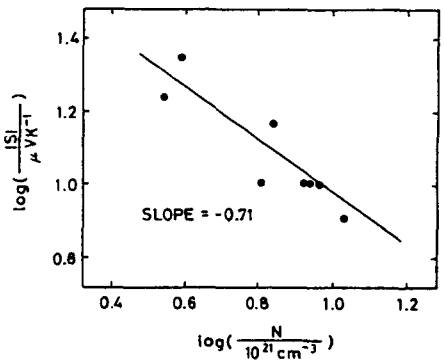

Fig.10. Seebeck coefficient of Eu_xNbO_3 (cubic) at 300 K vs. Nb^{4+} concentration

○ , $Eu_{0.52}NbO_{2.66}$
● , $Eu_{0.62}NbO_{2.70}$
□ , $Eu_{0.71}NbO_{2.82}$
■ , $Eu_{0.79}NbO_{2.93}$
△ , $Eu_{1.01}NbO_{3.01}$
▲ , $Eu_{0.90}NbO_{2.94}$

where d is the pycnometric density of the sample, L is Avogadro's number, M is the formula weight of the sample, and x and y are defined by the formula Eu_xNbO_y. The Seebeck coefficients for cubic Eu_xNbO_3 vary as $N^{-0.71}$ predicated by the free-electron model (Eq. 8). Therefore, the conduction electrons of cubic Eu_xNbO_3 are considered to be close to free electrons.

Figure 9 shows the Seebeck coefficient of Eu_xNbO_{2+x} at various temperature. Temperature dependence of the Seebeck coefficient for each Eu_xNbO_{2+x} is almost linear and this fact suggests that the behavior of the conduction electrons resemble that of the free electrons. The Seebeck coefficient of Eu_xNbO_{2+x} increases with decreasing x at each temperature (Fig. 9). The increase in the Seebeck coefficient means that the effective mass of the electrons of Eu_xNbO_{2+x} increases with decreasing x.

The effective masses of electrons for cubic Eu_xNbO_3 and Eu_xNbO_{2+x} are roughly evaluated by a thermoelectric power measurement, assuming that all the 4d electrons of niobium are concerned to the electrical conduction. The effective mass is obtained by comparison of the observed Seebeck coefficient with the calculated value ($m^* = m_o$).

In Table 2, effective electric masses of Eu_xNbO_3 and Eu_xNbO_{2+x} are listed. The effective electric mass for Eu_xNbO_{2+x} increases with decreasing x from $2m_o$ to $5m_o$. However, the effective mass for Eu_xNbO_3 is independent of x and about $2m_o$ for any sample obtained.

An interpretaion for the disagreement in masses of Eu_xNbO_{2+x} and Eu_xNbO_3 is as follows. The host lattice of Eu_xNbO_3, namely NbO_3, where the conduction electrons go through, is not changed

with x, and the effective mass is not affected by x. On the other hand, Eu_xNbO_{2+x} has oxygen vacancies, and the lattice of Eu_xNbO_{2+x} is fairly different from that of Eu_xNbO_3 at low x. The conduction electrons are trapped near the oxygen vacancies through the electrostatic force; the electrostatic interaction of the electrons with the vacancies is strong at low x, because there exist many oxygen vacancies at low x. This is the reason why the effective mass of the electrons for Eu_xNbO_{2+x} increases with decreasing x.

The resistivity of a metallic compound can be separated into two components. One of them is a residual component ρ_o which is ascribed to electron scattering by impurities and the scattering is temperature independent. The other one, ρ_T, is temperature dependent and is due to electron scattering by lattice vibrations. The total resistivity is therefore the sum of the temperature-independent, or residual, and the temperature-dependent, or thermal, components.

$$\rho = \rho_o + \rho_T \tag{10}$$

Figure 11 shows the drift residual mobilities as a function of europium concentration for cubic Eu_xNbO_3. On determination of the drift mobility, the carrier concentration is assumed to be equal to the Nb^{4+} concentration and is derived from Eq. 9. The drift mobility is calculated from following relation.

$$\mu_o = 1/Ne\rho_o \tag{11}$$

The drift residual mobility decreased with increasing europium concentration of x = 0.68-0.92 except for a range

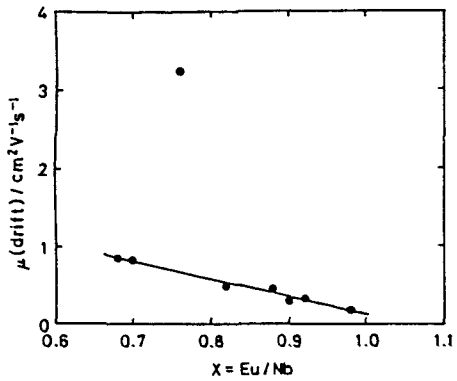

Fig.11. Drift residual mobility vs. composition (x) for Eu_xNbO_3

around x = 0.75. At x = 0.75 an irregularly high value was found. The values of mobility for these samples are considerably lower than the value for single crystals of other metallic compounds, e.g., Na_xWO_3 [29-31]. A degree of sintering will be a dominant factor for determining the value, and the degree is considered to decrease with europium concentration. An irregularly high mobility at x = 0.7 was also found in the studies of Na_xWO_3 [31,50,51]. Ellerbeck et al. [32] pointed out that the electrical homogeneity of the sample was an influential factor in the value of mobility and showed that there was no minimum in resistivity near x = 0.7 for electrically homogeneous Na_xWO_3. The homogeneity of the sample is an important factor for determining the value of resistivity, and the homogeneity should be maximum at x = 0.76.

Figure 12 shows the temperature dependence of the thermal part for $Eu_{0.76}NbO_{3.03}$. The thermal part of the resistivity is proportional to $T^{3.5}$ below 49 K, indicating that the mobility

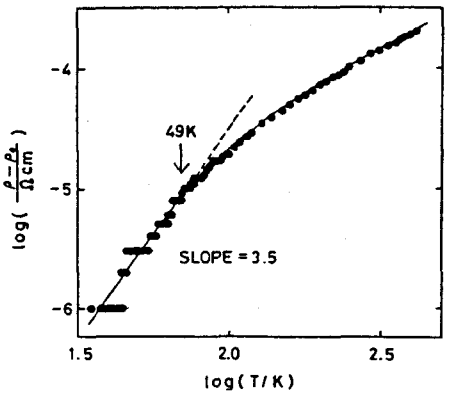

Fig.12. Temperature dependence of the thermal part of reistivity for $Eu_{0.76}NbO_{3.03}$

of electrons increases proportional to $T^{-3.5}$. Bardeen and Shockley [52] have proved that the mobility follows $T^{-1.5}$ dependence when the conduction electrons are scattered by the lattice vibrations for an acoustic mode. On the other hand, Greener et al. [53] suggest that a mobility of a polar semiconductor, in which the conduction electrons are scattered by the optical mode lattice vibrations, can be approximated by the relation at low temperature:

$$\mu = T^{-n}, \tag{12}$$

where n is a constant of magnitude 2-3.5. It is apparent that the conduction electrons of the niobium bronze are scattered by the optical mode lattice vibrations.

The interaction between electron and phonon is describable

by the perturbation theory of Howarth and Sondheimer [54] in which the conduction electrons were assumed to degenerate and to be scattered by polarization waves in the crystal. Crowder and Sienko [49] successfully applied the perturbation theory to the tungsten bronze. The thermal part of the electrical resistivity for the metallic compound is given in the relation:

$$\rho_T = AT^{-1}\sinh^{-2}(\Theta_D/2T), \tag{13}$$

where A is a constant and Θ_D is the Debye factor. The Debye temperature is conventionally estimated by a method proposed by Kunder and Sienko [55]. That is the transition temperature of resistivity from T^n to T^1 dependence in the resistivity curve (Fig. 12) is approximately $\Theta_D/7$. The constant A is evaluated from the measured value of the thermal part at 250 K and from an estimated Θ_D. The Debye temperature and the constant are

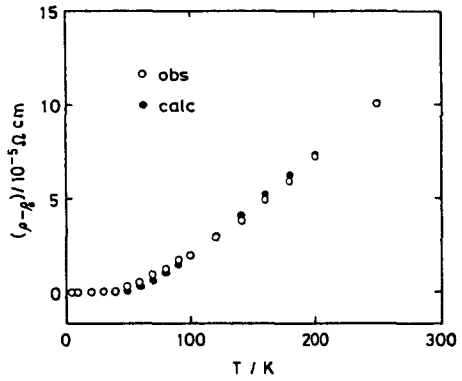

Fig.13. Comparison of the observed thermal part of resistivity with the calculated one

evaluated as 343 K and 1.41×10^{-2} ohm·K, respectively.

Figure 13 shows the results. The agreement between the observed and calculated values is satisfactory. The conduction manner in the bronze having some oxygen vacancies ($2+x < y < 3$) is essentially the same as in Eu_xNbO_3.

b. $EuNbO_z$ System

Phases

The total oxygen contents of the niobate were controlled by regulating the use of the reducing agent, Nb metal, in the preparative procedure. The O/Nb ratio of the samples was changed from 2.55 to 3.24.

An x-ray analysis revealed that the samples with a high oxygen content (O/Nb > 3) consist of Eu_xNbO_3 (major phase) and Eu_3NbO_6 (minor phase) (Table 3).

On the other hand, a cubic phase (lattice constant a = 4.131 Å) was found as a minor phase and Eu_xNbO_3 as major phase in the samples of low oxygen content. The intensity of the x-ray powder diffraction of the cubic phase increased with this ratio. At O/Nb = 2, the x-ray diffraction patterns of Eu_xNbO_3 disappeared, and the single phase of the cubic phase was obtained. The lattice constant of the cubic phase is 4.210 Å. Later, properties of the cubic phase is discussed.

Electrical Properties

Figure 14 shows the thermal coefficient of resistivity for the niobate at 300 K as a function of the oxygen content. The thermal coefficient decreases with increasing O/Nb ratio in the

Table 3. Analytical and magnetic data for the niobates with various oxygen contents

Exp. No.	Eu_xNbO_z (found) x	z	Eu_xNbO_z (nominal) x	z	$\frac{\mu_{eff}}{\mu_B}$ (found)	$\frac{\mu_{eff}}{\mu_B}$ (calcd)[a]	Phases
N	0.97	2.55	1.00	3.00	7.77	8.32	Eu_xNbO_3 + $EuNbO_2$
O	0.98	2.75	1.00	3.00	7.73	8.36	Eu_xNbO_3 + $EuNbO_2$
P	0.90	2.92	1.00	3.00	7.65	7.72	Eu_xNbO_3
Q	1.00	3.01	1.00	3.00	7.92	8.13	Eu_xNbO_3
R	0.90	3.10	1.00	3.00	7.42	7.65	Eu_xNbO_3 + Eu_3NbO_6
S	0.92	3.13	1.00	3.00	7.58	7.73	Eu_xNbO_3 + Eu_3NbO_6
T	0.97	3.24	1.00	3.00	7.75	7.91	Eu_xNbO_3 + Eu_3NbO_6

a: $\mu_{eff}(\text{calcd}) = \sqrt{x\mu^2(Eu^{2+}) + (Nb^{2+}/Nb)\mu^2(Nb^{2+}) + (Nb^{4+}/Nb)\mu^2(Nb^{4+})}$

$\mu(Eu^{2+}) = 7.94\ \mu_B$, $\mu(Nb^{2+}) = 3.87\ \mu_B$, $\mu(Nb^{4+}) = 1.73\ \mu_B$

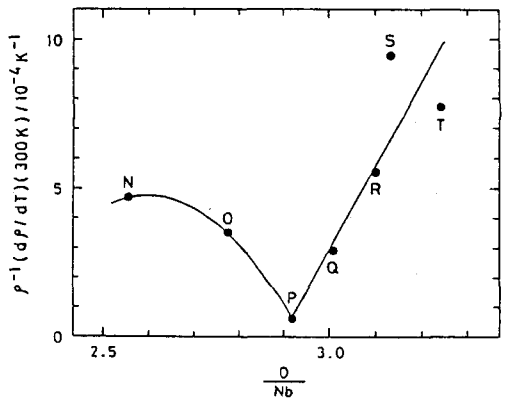

Fig.14. Thermal coefficient of electrical resistivity vs. oxygen content for the niobates. Symbols in the diagram are experimental number in Table 3

low-oxygen region (O/Nb < 2.9), while it increases with the oxygen content in the high-oxygen region (O/Nb > 2.9). In other words, the thermal coefficient increases with the amount of the second phase, i.e., Eu_3NbO_6 and $Eu_{0.5}Nb_{0.5}O$ in the range $2.55 < O/Nb < 3.24$.

Figure 15 shows a composit plot of electrical resistivity versus temperature for several sintered samples. The appropreate compositional data for these samples are tabulated in Table 3. The electrical resistivity curve of the niobate with a high oxygen content (O/Nb > 3)shows two distinct regions: (1) less than 55 K a broad peak, being maximum at 9 K, is observed in the resistivity curve around 7 K to 55 K; and (2) above 55 K the resistivity rises slowly with temperature.

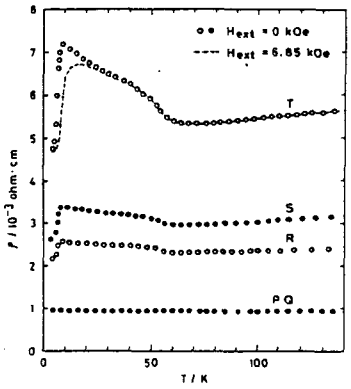

Fig.15. Resistivity vs. temperature for the niobates. Symbols in the diagram are experimental numbers in Table 3

However, there exists no peak in the resistivity curve for samples that are stoichiometric or low in oxygen content.

A similar behavior has been reported for EuO, EuS, and EuSe, and it is concluded that a magnetic interaction of Eu^{2+} causes the effects. Magnetic measurements show that the sample with a high oxygen content has a ferromagnetic Curie point at 7 K and $4f^7$ spin of Eu^{2+} ordered below the temperature. This point is two degrees lower than the temperature T_m at which the zero-field resistivity is maximum for each sample with a high oxygen content. The resistivity peak near the Curie temperature was observed for the samples with a high oxygen content and could not be found for the samples that were stoichiometric or low in oxygen content (Fig. 15).

The observation suggests that a second phase appearing in a high oxygen content region indirectly affects the conduction electrons of Eu_xNbO_3 magnetically. The phase of interest may be Eu_3NbO_6 with oxygen vacancy or trace amount of Eu_3O_4.

In Eu_xNbO_3, the Eu^{2+} - Eu^{2+} nearest neighbor distance is so long that the Eu^{2+} cannot interact magnetically, and no peak was observed in the resistivity curve of Eu_xNbO_3 (Q) and Eu_xNbO_3 with oxygen vacancy (P). Therefore, an indirect and magnetic interaction between Eu_xNbO_3 and the second-phase was assumed to exist in order to explain the appearence of the resistivity peak.

The influence of EuO on the resistivity peak can be neglected in this case, since EuO has a high ferromagnetic Curie point at 69 K and is known to have a resistivity peak mamimum at 80 K.

One of the most important methods to judge whether the peaks are caused by the magnetic interaction is to measure the resistivity in an external magnetic field H_{ext}. The electrical resistivity of sample "T" was therefore measured in a magnetic field of 6.85 kOe from 4.2 K to 77.4 K (a dashed line in Fig. 15).

Figure 15 shows that the magnitude of the resistivity peak decreases, T_m shifts from 9 K to 16 K, and the onset of the sharp resistivity rise shifts from 4 K to 6 K with the external magnetic field.

All these phenomena are very analogous to those of EuO [56,57], and lead to the assumption that the mechanism of the resistance resembles to that of EuO [56-59].

In the theories of de Gennes and Friedel [57,60], and of

Kim [57,61], in which the magnetic scattering of electrons is assumed to be dominated by long-range spin fluctuations, the peak of inverse electronic mobility μ^{-1} is exactly at T_C.

On the other hand, Fisher and Langer [57,62] have shown that the peak in the reciprocal mobility μ^{-1} occurs at $T > T_C$, when the magnetic scattering of electrons is dominated by short-range spin fluctuations.

In our case, T_m is two degrees higher than T_C. When the number of conduction electrons is, hypothetically, assumed to be unchanged, the latter process must be dominant in the samples with a high oxygen content.

c. $Eu(II)_xNb(II)_{1-x}O$ System

Phases

The phase and analytical data for $Eu_xNb_{1-x}O$ obtained are shown in Table 4. Single phases are obtained at x = 0.33 and 0.5. One of the single phases, $Eu_{0.33}Nb_{0.67}O$, is purple tinged dull blue polycrystal, and has a grayish blue color and a cubic lattice with a = 4.135 Å.

Syntheses of analogs, $Sr_{0.33}Nb_{0.67}O$ and $Sr_{0.5}Nb_{0.5}O$, were attempted. The mixtures of $SrCO_3$ and Nb_2O_5 were subjected to the solid state reaction in a flow of H_2 at 1623 K for 20 h. The reducing power of H_2 was not strong enough to convert Nb_2O_5 to NbO, and a great amount of NbO_2 was found in the product. Therefore, $Sr_xNb_{1-x}O$ could not be obtained in this manner. Syntheses of mixed oxides, $Sr_xNb_{1-x}O$, were hence tried by the reaction of $SrCO_3$ and NbO under continuously pumped vaccum

Table 4. Analytical data for $Eu(II)_xNb(II)_{1-x}O$

$Eu_xNb_{1-x}O_y$ (Nominal)		$Eu_xNb_{1-x}O_y$ (Analytical)		Phase	a / Å	ρ/g·cm^{-3}
x	y	x	y			
0.13	1.00	0.14	0.97	(1) + NbO	-	-
0.25	1.00	0.26	1.01	(1) + NbO	-	-
0.33	1.00	0.33	1.08	(1)	4.019	7.51
0.40	1.00	0.38	1.00	(1) + (2)	-	-
0.50	1.00	0.49	1.08	(2)	4.135	7.65
0.75	1.00	0.72	1.20	(2) + EuO	-	-

(1) $Eu_{0.33}Nb_{0.67}O$; (2) $Eu_{0.5}Nb_{0.5}O$

(10^{-3} Pa). A purple single phase of $Sr_{0.33}Nb_{0.67}O$ was obtained. However, a single phase of $Sr_{0.5}Nb_{0.5}O$ was not given and a mixture of $Sr_{0.5}Nb_{0.5}O$ and $Sr_{0.33}Nb_{0.67}O$ was obtained. An excess of $SrCO_3$ was required to prepare the Sr analog of $Eu_{0.5}Nb_{0.5}O$. At the nominal composition of $Sr_{0.6}Nb_{0.4}O$, the Sr analog of $Eu_{0.5}Nb_{0.5}O$ was detected in the powder x-ray pattern. However, $Sr_{0.6}Nb_{0.4}O$ may be the mixed phase of the Sr analog of $Eu_{0.5}Nb_{0.5}O$ and amorphous SrO, since $Sr_{0.6}Nb_{0.4}O$ is hygroscopic. The single phase of the Sr analog of $Eu_{0.5}Nb_{0.5}O$ was not prepared even in the reaction of $SrCO_3$ and NbO.

Electrical Properties

Electrical resistivity measurements were done for $Eu_{0.33}Nb_{0.67}O$, $Eu_{0.5}Nb_{0.5}O$, and $Sr_{0.33}Nb_{0.67}O$ (Figs. 16 and 17). Resistivities of $Eu_{0.33}Nb_{0.67}O$ and $Sr_{0.33}Nb_{0.67}O$ are very low at room temperature and the thermal coefficients of resistivity for these compounds are positive, indicating that these are metallic

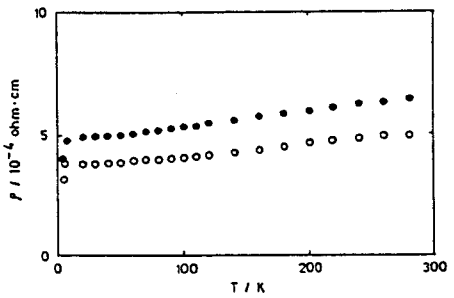

Fig.16. Electrical resistivity vs. temperature for $Eu_{0.33}Nb_{0.67}O$ (●) and $Sr_{0.33}Nb_{0.67}O$ (○)

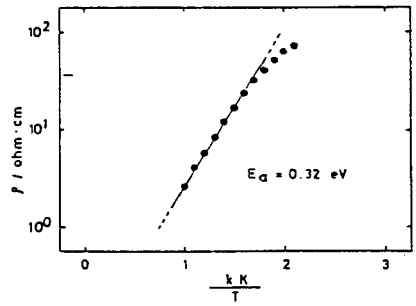

Fig.17. Electrical resistivity vs. inverse temperature for $Eu_{0.5}Nb_{0.5}O$

conductors (Fig. 16). On the other hand, $Eu_{0.5}Nb_{0.5}O$ is a typical semiconductor (Fig. 17), and its temperature dependence of resistivity is expressed by the well-known relationship:

$$\rho = \rho_o \exp(E_a/kT). \qquad (14)$$

The activation energy (E_a) for $Eu_{0.5}Nb_{0.5}O$ was 0.32 eV. These resistivity data indicate that 4d electrons of niobium are

collective for $Eu_{0.33}Nb_{0.67}O$ and $Sr_{0.33}Nb_{0.67}O$, and localized for $Eu_{0.5}Nb_{0.5}O$.

Magnetic Properties

Magnetic susceptibility measurements were done for $Eu_{0.33}Nb_{0.67}O$, $Eu_{0.5}Nb_{0.5}O$, $Sr_{0.33}Nb_{0.67}O$, and $Sr_{0.6}Nb_{0.4}O$ (Table 5). The magnetic data show that $Eu_{0.33}Nb_{0.67}O$ and $Eu_{0.5}Nb_{0.5}O$ are paramagnetic substances, and $Sr_{0.33}Nb_{0.67}O$ and $Sr_{0.6}Nb_{0.4}O$ are a Pauli paramagnetic and a diamagnetic substances respectively. The magnetic data for $Sr_{0.33}Nb_{0.67}O$ indicate that there is no unpaired Nb4d spin. Paramagnetic properties of $Eu_{0.33}Nb_{0.67}O$ and $Eu_{0.5}Nb_{0.5}O$ are arised from paramagnetic Eu^{2+} ions. The observed magnetic moments of $Eu_{0.33}Nb_{0.67}O$ and $Eu_{0.5}Nb_{0.5}O$ agree closely with the calculated values, which are derived on the assumption that all the 4d spins are paired. The good agreements between the observed and the calculated values indicate that all the europium ions are in a bivalent state and that there is no unpaired Nb4d spin. The diamagnetic properties

Table 5. Electrical and magnetic data for $Eu(II)_xNb(II)_{1-x}O$ and $Sr(II)_xNb(II)_{1-x}O$

Compound	Electrical Property	Ea/ev[a)]	Magnetism	μ_{eff}/μ_B (Found)	μ_{eff}/μ_B [b)] (Calcd)	χ_g(300K) $emu \cdot g^{-1}$
$Eu_{0.33}Nb_{0.67}O$	metallic	-	para	4.70	4.56	$7.4X10^{-5}$
$Eu_{0.5}Nb_{0.5}O$	semiconductive	0.32	para	5.30	5.61	$8.8X10^{-5}$
$Sr_{0.33}Nb_{0.67}O$	metallic	-	Pauli-para	-	-	$8X10^{-10}$
$Sr_{0.6}Nb_{0.4}O$	semiconductive	-	dia	-	-	$< 10^{-10}$

a) Ea is activation energy in a equation; $\rho = \rho_o \exp(Ea/kT)$

b) $\mu_{eff}(Calcd) = \sqrt{x}\,\mu(Eu^{2+})$; $\mu(Eu^{2+}) = 7.94\ \mu_B$

of the Sr analogs also support the assumption that all the 4d spins are paired in the Eu compounds. The metallic conduction and Pauli paramagnetism of $Sr_{0.33}NbO_{0.67}$ ($Eu_{0.33}NbO_{0.67}$ analog) suggest that the Nb4d electrons exist as conduction electrons in $Eu_{0.33}NbO_{0.67}$. Similarly, the semiconduction and diamagnetic properties suggest that the Nb4d electrons are paired in $Eu_{0.5}NbO_{0.5}$.

1-4. Summary

The structural and the electrical properties of the europium niobium bronzes with various europium and oxygen compositions (Eu_xNbO_y) have been investigated. The results obtained in this chapter are as follows.

1. Mixed oxides containing bivalent europium, Eu_xNbO_y, were synthesized by the solid state reaction of Eu_2O_3, Nb_2O_5, and Nb powder. A niobium bronze with a stoichiometric oxygen content, namely y = 3, was in tetragonal form for x = 0.5-0.65 and in cubic form for x = 0.65-1.00. A niobium bronze with full oxygen vacancies, Eu_xNbO_{2+x} where all europium and niobium ions were in bivalent and tetravalent states respectively, crystallized in cubic form in the single phase region ($0.5 < x < 1.0$).

2. The cubic niobium bronze of any composition between y = 3 and 2+x exhibited metallic conduction and the tetragonal bronze was a semiconductor. A Goodenough model for the tungsten bronze, Na_xWO_3, was employed for the difference in the electrical

conduction behavior among cubic Eu_xNbO_3 and Eu_xNbO_{2+x} and tetragonal Eu_xNbO_3. Residual drift mobility for cubic Eu_xNbO_3 decreased with x except for x = 0.76 and on this point an irregularly high value was obtained. The temperature-dependent part of the drift mobility for the cubic one was found to be describable by the perturbation theory of Howarth and Sondheimer. Thermoelectric power measurements showed that the charge carriers of each bronze were electrons. An effective mass of the electron for each cubic Eu_xNbO_3 was about $2m_o$ (m_o was the electronic rest mass), and the quasi-free electron model was roughly applicable. However, the effective mass of electron for cubic Eu_xNbO_{2+x} increased with decreasing x from $2m_o$ to $5m_o$.

3. Thermal coefficients of electrical resistivity for the niobates with various oxygen contents were all positive in the range y = 2.55-3.24 and exhibited a sharp minimum at O/Nb = 2.92. In all these niobates, Eu_xNbO_3 was a major phase and Eu_3NbO_6 or $Eu_{0.5}Nb_{0.5}O$ was detected as a second phase in the range O/Nb > 3 or O/Nb < 3 respectively. Peaks in the resistivity curves were correlated with a magnetic ordering temperature for samples with an overall ratio O/Nb > 3.

4. Two new compounds, $Eu_{0.33}Nb_{0.67}O$ and $Eu_{0.5}Nb_{0.5}O$, were found in the ternary system $Eu(II)_xNb(II)_{1-x}O$. Electrical resistivity measurements showed that $Eu_{0.33}Nb_{0.67}O$ was a metallic conductor while $Eu_{0.5}Nb_{0.5}O$ was a semiconductor. Strontium analogs of these compounds, $Sr_{0.33}Nb_{0.67}O$ and $Sr_{0.5}Nb_{0.5}O$, were also attempted to be prepared. The former was obtained as a single phase.

Chapter 2

OXIDATION OF EUROPIUM (II) NIOBIUM BRONZES

2-1. Introduction

In the foregoing chapter, electrical properties of the europium niobium bronze have been examined, and it is found that the thermal coefficient of the electrical resistivity for the cubic bronze is very low at specific compositions. This property is desirable for an electrical resistor material. However, bivalent europium ions in a mixed oxide are easily oxidized by the atmospheric oxygen at high temperatures. It is necessary to know that at what temperature the niobium bronzes are oxidized. The oxidation mechanisms of the bronze have also attracted our attention, because the cubic and the tetragonal bronzes undergo in different ways. Krylov et al. [47] have reported that $EuNbO_4$ is an oxidized product of $EuNbO_3$. However, oxidation products and oxidation mechanism of Eu_xNbO_3 have not been reported. In this chapter, oxidation of Eu_xNbO_3 is discussed.

2-2. Experimental

Magnetic Measurements

The magnetic susceptibilities of Eu_xNbO_3 were measured under an air atmosphere from 300 K to 1173 K at a heating rate of 10 K/min, using a Shimadzu magnetic balance "MB-11".

Thermal Measurements

Differential thermal analysis (DTA) and thermogravimetric analysis (TGA) were carried out in the air at a heating rate of 10 K/min in the temperature range 300-1173 K. All thermal measurements were performed on a Rigaku Denki DTA "Thermoflex". Powder samples (30-60 mg) were used, alumina powder (99.9%) being employed as a reference. The heat of oxidation for the bronzes was measured with a differential scanning calorimeter (DSC). Measurements were carried out in the air at a heating rate of 10 K/min in the temperature range 300-1173 K. The heat of oxidation was determined from the area beneath a DSC peak. The heat of oxidation of NbO_2 to Nb_2O_5 was used as a standard [63].

2-3. Results and Discussion

Typical TGA and DTA curves for tetragonal and cubic Eu_xNbO_3 are shown in Fig. 18. An abrupt weight gain is observed in the TGA curve for tetragonal Eu_xNbO_3 at 550-700 K, and a moderate weight gain at 550-900 K for the cubic one. We see that the oxidation proceeds in two steps for both the tetragonal

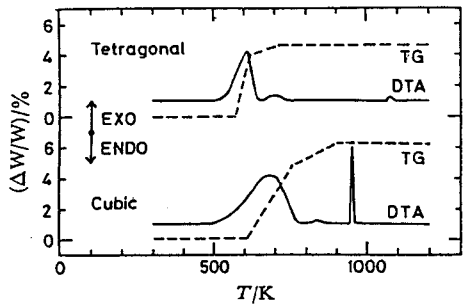

Fig.18. TGA and DTA curves of $Eu_{0.51}NbO_{2.98}$ (tetragonal) and $Eu_{0.74}NbO_{7.43}$ (cubic)

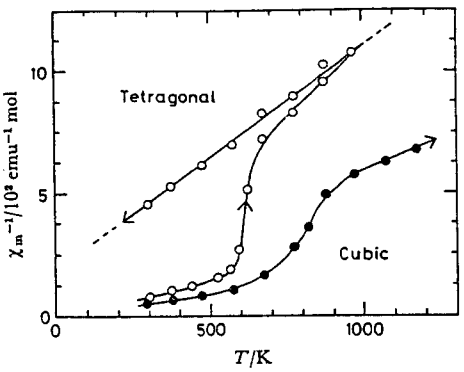

Fig.19. Inverse magnetic susceptibility vs. temperature for $Eu_{0.51}NbO_{2.98}$ (tetragonal) and $Eu_{0.74}NbO_{2.81}$ (cubic)

and the cubic bronzes.

Magnetic susceptibility measurements were carried out for the same samples in the air in the temperature range 300-1173 K, at a heating rate of 10 K/min (Fig. 19). The magnetic moments of Eu^{2+}, Eu^{3+}, Nb^{4+}, and Nb^{5+} are 7.94, 3.4, 1.73, and 0 μ_B, respectively. The decrease in the magnetic moment is much

larger in the oxidation of Eu^{2+} to Eu^{3+} than in the oxidation of Nb^{4+} to Nb^{5+}. From a comparison of the TG-DTA curves (Fig. 18) with the χ_m^{-1} vs. T curves (Fig. 19), we see that the initial stage of the oxidation would be due to the oxidation of Eu^{2+}, the second to the oxidation of Nb^{4+}. Figure 19 also shows that the initiating temperature of the oxidation of Eu^{2+} is 550 K for both the tetragonal and cubic bronzes, the rate of oxidation of Eu^{2+} being larger for the tetragonal bronze than for the cubic one.

The stability of the bronze against oxidation mainly depends on that of Eu^{2+}. The temperature at which oxidation of Eu^{2+} starts is the same for both the tetragonal and cubic bronzes. The stability of Eu^{2+} to oxidation seems to be the same order for both bronzes. The rate of oxidation of Eu^{2+} is considered to determine the rate of oxidation of the bronzes.

The thermal analyses (TGA and DTA) were carried out for EuO under the same conditions as those for the bronzes. EuO oxidized at 520-580 K, showing that the rate of oxidation of Eu^{2+} in EuO is much greater than that in the bronzes. The oxidation of Eu^{2+} proceeds form the surface to the bulk of the bronze grain. The rate of oxidation of Eu^{2+} in the bulk should be determined by the probability of Eu^{2+} encounter with oxygen. Thus the rate of diffusion of oxygen in the oxidized product layer should control the rate of oxidation of Eu^{2+}.

X-Ray analysis was carried out for the bronzes oxidized at various temperatures. Oxidation of the cubic bronze gave an amorphous phase crystallizing at 950 K. On the other hand, the tetragonal phase underwent oxidation giving complex

crystalline products which recrystallized at 1070 K. The difference in the rate of oxidation between the tetragonal and cubic bornzes can be attributed to the difference in the rate of diffusion on oxygen in the layer of the oxidized product. The diffusion coefficient of oxygen for the product obtained by the oxidation of the tetragonal phase should be much larger than for the amorphous phase resulting from the cubic phase.

On heating the bronzes in the air, $EuNbO_4$ appeared at 1070 K for the tetragonal bronze and at 950 K for the cubic bornze. Exothermic peaks, 950 K and 1070 K, due to crystallization are seen in the DTA curves with no weight change (Figs. 18 and 20), suggesting that the amorphous phases are less stable than the crystalline phases. The difference in the stability of the

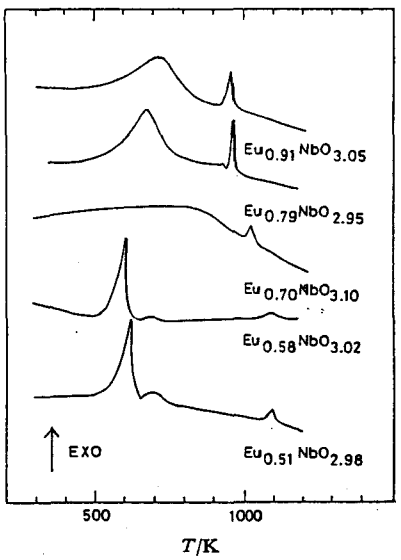

Fig.20. DTA curves for Eu_xNbO_3

intermediate states affects the heats of oxidation for these bronzes.

Figure 21 shows the observed and calculated heats of oxidation for the bronzes of various Eu^{2+} contents. The observed heat of oxidation shows a minimun at x = 0.65. For the evaluation of the heat of oxidation, the bronze is assumed to be a mixture of EuO, NbO_2, and Nb_2O_5.

$$Eu_xNbO_y = xEuO + (2x-2y+5)NbO_2 + (y-x-2)Nb_2O_5 \qquad (15)$$

The oxidation reaction is assumed to proceed as follows:

$$Eu_xNbO_y + (0.75x-0.5y+1.25)O_2 \longrightarrow 0.5xEu_2O_3 + 0.5Nb_2O_5. \qquad (16)$$

The minimum of the heat of oxidation at x = 0.65 corresponds to the phase transition.

The heat of oxidation for the tetragonal bronze are almost

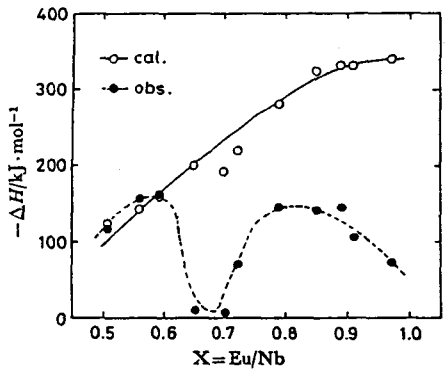

Fig.21. Heat of oxidation for Eu_xNbO_3

equal to the calculated values. The result indicates that the heat of formation for the cystalline phase is close to that for the mixture of Eu_2O_3 and Nb_2O_5 represented by Eq. 16. The heat of transformation from an unknown crystalline phase to the final products, mainly $EuNbO_4$, as well as $EuNb_3O_9$ and $EuNb_5O_{14}$, might be very small. Thermal analyses (TGA-DTA) support the assumption.

The heat of oxidation for the cubic bronzes is much lower than that for the calculated ones, a minimum being obtained at $x = 0.65$. The result indicates that the heat of formation for the amorphous phase is considerably larger than that for the mixture of Eu_2O_3 and Nb_2O_5 shown in Eq. 16. The minimum of the heat of oxidation at $x = 0.65$ is due to the difference in stability of these two intermediate phases.

2-4. Summary

The oxidation mechanism of Eu_xNbO_3 was investigated. The results obtained in this chapter are as follows.

1. The bivalent europium ions in the cubic and the tetragonal bronzes were oxidized by the atmospheric oxygen over 550 K.
2. The europium bronzes were oxidized in two steps. One of them was the oxidation of Eu^{2+} and the other was that of Nb^{4+}.
3. The oxidation mechanism of the cubic bronze differed from that of the tetragonal bronze, the cubic bronze giving an amorphous phase and the tetragonal bronze complex crystalline products. The oxide, $EuNbO_4$, was crystallized from both the

amorphous and crystalline phases at 950 K and 1070 K, respectively. TG-DAT and magnetic studies indicated that the oxidized phases played an important role in the rate-determining step of oxidation for the bronzes.

Chapter 3

PREPARATION AND ELECTRICAL PROPERTIES OF SINTERED $EuZrO_3$ - $EuNbO_3$ AND $EuTiO_3$ - $EuNbO_3$

3-1. Introduction

Perovskite type oxides containing the bivalent europium $EuMO_3$ [20,21] are of great interest for their electrical and magnetic properties. These properties, especially electrical conduction, are very sensitive to the crystal system and to the kind of metal occuping the B site of $EuMO_3$. For example, cubic perovskite $EuNbO_3$ exhibits metallic conduction while similar products $EuZrO_3$ and $EuTiO_3$ are semiconductor [23]. It was expected that $EuNbO_3$ could be sintered with $EuZrO_3$ or $EuTiO_3$ since these perovskites were in the same crystal system [20,21,23,24] and the ionic radius [37] of Nb^{4+} (0.74 Å: 6th-fold coordination)was close to that of Zr^{4+} (0.79 Å: 6th-fold coordination) or to that of Ti^{4+} (0.61 Å: 6th-fold coordination). Furthermore, the electrical properties of the sintered material were expected to be between $EuNbO_3$ with $EuZrO_3$ or $EuTiO_3$. The object of our study was to sinter $EuNbO_3$ with $EuZrO_3$ or with $EuTiO_3$ to develop a new type of resistor having the following

two properties.

(1) Controlled value of resistivity.

(2) Controlled thermal coefficient of resistivity.

In this chapter, electrical properties of sintered $EuZrO_3$ - $EuNbO_3$ and $EuTiO_3$ - $EuNbO_3$ are discussed.

3-2. Experimental

a. $EuZrO_3$ - $EuNbO_3$ System

Preparation

A miture of Eu_2O_3, ZrO_2, Nb_2O_5, and Zr or Nb powder was ground together in an agate mortar and pressed into pellets. They were packed into a molybdenum box, sealed under vacuum (10^{-3} Pa) in a silica capsule and heated at 1423 K for 50 h. The reaction was assumed to occur according to the reaction:

$$0.5Eu_2O_3 + aZrO_2 + bNb_2O_5 + cZr \text{ or } dNb \longrightarrow yEuZrO_3 + (1-y)EuNbO_3. \quad (17)$$

A small amount of oxygen was removed from the sintered product by means of an isopiestic technique [65] in which the compound was encapsulated in a silica tube with a quantity of Nb metal held at 1273 K for 30 h.

Analyses

The phase purities and structural type of the sintered samples were characterized by x-ray powder analysis with a Rigaku Denki Rotor-flex diffractometer. The atomic ratio (Eu:Zr:Nb) was determined with a Rigaku Denki energy dispersion

type x-ray fluorescent spectrograph unit, Ultra trace system. The oxygen compositional states of the samples were determined by weighing the samples before and after complete oxidation at 1100 K in air and assuming that all of the detectable weight gain was due to the reaction:

$$Eu_xZr_yNb_{1-y}O_z + aO_2 \longrightarrow 0.5xEu_2O_3 + yZrO_2 + 0.5(1-y)Nb_2O_5, \quad (18)$$

where x and y were Eu and Zr contents determined by the x-ray fluorescent analysis. The magnetic moment of the samples was obtained with a Shimadzu magnetic balance "MB-11".

Electrical Resistivity Measurements

Electrical resistivity measurements were performed on sintered polycrystalline pellets. The pellets were prepared by pressing the powder samples and then sintering them at 1473 K for 10 h in sealed silica capsules.

The electrical resistivity measurement for the sintered samples was carried out in a helium atmosphere from 4.2 to 1000 K. A simple four-probe d.c. method was employed for the resistivity measurement. The measurement was performed in the potential region in which the sample behaved ohmically. Furthermore, to avoid any contribution to the measured potential from thermally generated emf's, readings were taken in both forward and reverse directions, and the averaged values were recorded.

b. $EuTiO_3$ - $EuNbO_3$ System

Preparation

Europium niobium oxide, Eu_xNbO_3, and europium titanium

oxide, $EuTiO_3$, were used as starting materials. A mixture of $EuTiO_3$ and $EuNbO_3$ was ground together in an agate mortar and pressed into pellets. The pellets were packed into a molybdenum box, sealed under vacuum (10^{-3} Pa) in a silica capsule after degassing at 473 K, and heated at 1453 K for 10 h. The starting materials, $EuTiO_3$ and $EuNbO_3$, were synthesized by a solid state reaction of Eu_2O_3, Nb_2O_5, TiO_2, Ti, and Nb. The reaction is as follows.

$$0.5Eu_2O_3 + 0.75TiO_2 + 0.25Ti \longrightarrow EuTiO_3 \qquad (19)$$

$$0.5Eu_2O_3 + 0.3Nb_2O_5 + 0.4Nb \longrightarrow EuNbO_3 \qquad (20)$$

Analyses

An x-ray powder analysis was done for characterizing the phase purity and structure of the sintered samples with a Rigaku Denki Rotor-flex diffractometer. The atomic ratio (Eu:Ti:Nb) was determined with a Rigaku Denki energy dispersion type x-ray fluorescent spectrograph unit "Ultra trace system". The oxygen composition of the sintered sample was determined by weighing the sample before and after complete oxidation at 1100 K and by analyzed atomic ratio of metal. On evaluating the oxygen composition, the following oxidation reaction was assumed:

$$Eu_xTi_yNb_{1-y}O_z + (0.75x-0.25y-0.5z+1.25)O_2 \longrightarrow 0.5xEu_2O_3 + yTiO_2 + 0.5(1-y)Nb_2O_5, \qquad (21)$$

where x and y were the analyzed atomic ratio of Eu and Ti to the total metal amount (Ti+Nb) and z was an oxygen content.

The oxidation state of europium in the sintered product was analyzed by measuring the magnetic moment of the sample with a

Shimadzu mgnetic balance "MB-11".

Electrical Resistivity Measurements

An electrical resistivity measurement was done for the sintered polycrystal bar of about 0.05 cm^2 in cross section and 8 mm long. A standard four-probe method was used for the resistivity measurement of low resistivity samples and a two-probe method was employed for the measurement of high resistivity samples. The resistivity measurement was performed under a He atmosphere at low temperature and under vacuum at high temperature so as to avoid oxidation of the sample. To separate the measured potential from thermally generated emf's, the d.c. current was stopped at a 10 min interval and the drift of the zero current potential was checked.

3-3. Results and Discussion

a. $EuZrO_3$ - $EuNbO_3$ System

The sintered polycrystalline samples had a color varing from purple tinged blue (y = 0) to pale yellow (y = 1.0). An x-ray analysis revealed that the sintered samples consisted on Eu_xNbO_3 and $EuZrO_3$. No solid solution of $EuNbO_3$ and $EuZrO_3$ was observed.

The compositional and magnetic data for the sintered samples are given in Table 6. It is seen that each observed atomic ratio of Zr, Nb, and O for the samples is close to the calculated value, while the atomic ratio of Eu for the samples is somewhat lower than expected. This lowering means that europium is

Table 6. Analytical and magnetic data for $[yEuZrO_3 + (1-y)EuNbO_3]$

Exp. No.	$Eu_xZr_yNb_{1-y}O_z$ (found) x	y	z	$Eu_xZr_yNb_{1-y}O_z$ (calcd) x	y	z	$\frac{\mu_{eff}}{\mu_B}$ (found)	$\frac{\mu_{eff}}{\mu_B}$ (calcd)[a]	Phases
A	0.98	1.00	3.03	1.00	1.00	3.00	8.07	7.86	$EuZrO_3$
B	0.99	0.94	3.03	1.00	0.95	3.00	8.00	7.90	$EuZrO_3 + Eu_xNbO_3$
C	0.98	0.90	3.03	1.00	0.90	3.00	7.88	7.86	$EuZrO_3 + Eu_xNbO_3$
D	0.95	0.74	3.02	1.00	0.75	3.00	7.94	7.76	$EuZrO_3 + Eu_xNbO_3$
E	0.93	0.49	2.97	1.00	0.50	3.00	7.84	7.74	$EuZrO_3 + Eu_xNbO_3$
F	0.91	0.24	2.96	1.00	0.25	3.00	7.67	7.71	$EuZrO_3 + Eu_xNbO_3$
G	0.97	0.18	3.01	1.00	0.19	3.00	7.89	7.96	$EuZrO_3 + Eu_xNbO_3$
H	0.91	0.17	2.91	1.00	0.17	3.00	8.10	7.93	$EuZrO_3 + Eu_xNbO_3$
I	0.89	0.15	2.91	1.00	0.16	3.00	7.84	7.98	$EuZrO_3 + Eu_xNbO_3$
J	0.90	0.14	2.93	1.00	0.14	3.00	8.01	7.97	$EuZrO_3 + Eu_xNbO_3$
K	0.99	0.13	3.01	1.00	0.13	3.00	8.00	8.06	$EuZrO_3 + Eu_xNbO_3$
L	0.99	0.06	3.00	1.00	0.06	3.00	8.05	8.07	$EuZrO_3 + Eu_xNbO_3$
M	1.01	0.00	3.01	1.00	0.00	3.00	7.92	8.16	Eu_xNbO_3

a: μ_{eff} (calcd) $= \sqrt{x\mu^2(Eu^{2+}) + (Nb^{4+}/Nb)\mu^2(Nb^{4+})}$, $\mu(Eu^{2+}) = 7.94\ \mu_B$, $\mu(Nb^{4+}) = 1.73\ \mu_B$

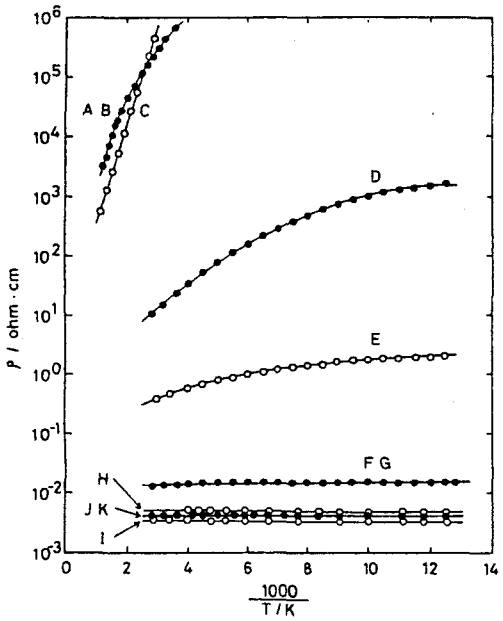

Fig.22. Resistivity vs. reciprocal temperature for $EuZrO_3$ - $EuNbO_3$. Symbols in the diagram are experimental numbers in Table 6

evaporated form the products as EuO at more than 1473 K.

The observed magnetic moments are in agreement with the calculated values, though a small lowering of the magnetic moment is found in the Nb rich samples. It is because the reduction power of niobium is not strong enough, compared with zirconium, to reduce all of Eu^{3+} in the starting material to Eu^{2+} [21].

The resistivity data for the two-phase sintered samples with various values of y are given in Fig. 22 as a function of the reciprocal temperature. The electrical resistivity for the samples of high y (y > 0.14) is a characteristic of a

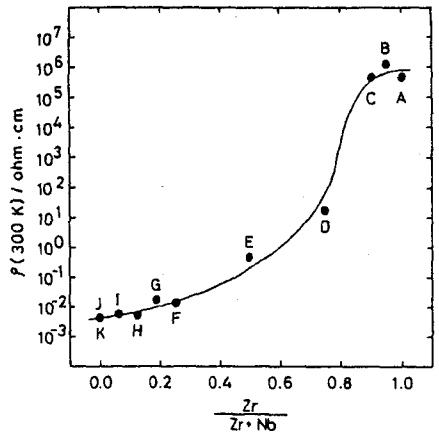

Fig.23. Resistivity at 300 K vs. Zr content for $EuZrO_3$ - $EuNbO_3$. Symbols in the diagram are experimental numbers in Table 6

semiconducting material, and that for the samples of low y ($y < 0.14$) is a property of a metallic one. An activation energy of conduction for $EuZrO_3$ approaches an intrinsic value of 0.13 eV at 800 K, and this means that the $4f^7$ level of Eu lies 0.13 eV below the bottom of the conduction band. The activation energy decreases with increasing proportion of Nb in the samples.

Figure 23 shows the resistivity data for the samples at 300 K as a function of y. The data reveals that the resistivity of the samples increases with y.

Figure 24 shows the thermal coefficient of resistivity for the samples at 300 K. The thermal coefficients vary from $+5.9 \times 10^{-4}\ K^{-1}$ to $7.4 \times 10^{-4}\ K^{-1}$. At $y = 0.14$, the thermal coefficient of resistivity is nearly zero.

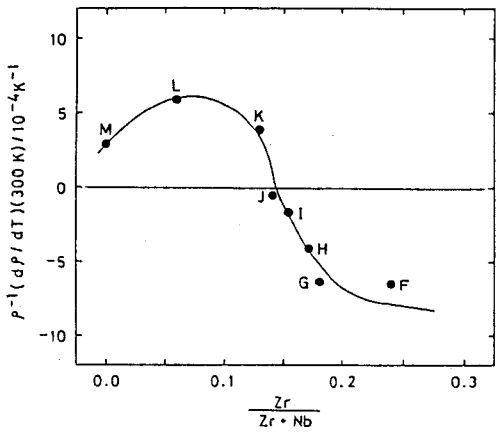

Fig.24. Thermal coefficient of resistivity vs. Zr content for $EuZrO_3$ - $EuNbO_3$. Symbols in the diagram are experimental numbers in Table 6

b. $EuTiO_3$ - $EuNbO_3$ System

Kasimov et al. [66] have been reported that solid solutions of $EuTiO_3$ and $EuNbO_3$ exist. However, we could not find any solid solution in the $EuTiO_3$ - $EuNbO_3$ system under our experimental conditions, in which $EuNbO_3$ was heated with $EuTiO_3$ at 1423 K for 10 h under vacuum, and two-phase sintered products of $EuTiO_3$ and $EuNbO_3$ were given. The sintered samples have a color varing from purple tinged blue (y = 0) to gray (y = 1).

The compositional and magnetic data of the sintered samples are listed in Table 7. The observed magnetic moment of the sintered products fits well with the calculated one, which is calculated by assuming that all europium ions of the products

Table 7. Analytical and magnetic data for $[yEuTiO_3 + (1-y)EuNbO_3]$

Exp. No.	$Eu_xTi_yNb_{1-y}O_z$ (found)			$Eu_xTi_yNb_{1-y}O_z$ (nominal)			$\frac{\mu_{eff}}{\mu_B}$	$\frac{\mu_{eff}}{\mu_B}$ [a]	Phases
	x	y	z	x	y	z	(found)	(calcd.)	
A	1.01	0.00	3.01	1.00	0.00	3.00	7.94	7.98	$EuNbO_3$
B	0.98	0.14	3.09	1.00	0.13	3.00	7.93	7.86	$EuNbO_3 + EuTiO_3$
C	0.96	0.25	3.06	1.00	0.25	3.00	7.94	7.80	$EuNbO_3 + EuTiO_3$
D	0.99	0.38	3.09	1.00	0.38	3.00	8.00	7.91	$EuNbO_3 + EuTiO_3$
E	1.01	0.50	3.10	1.00	0.50	3.00	8.07	7.99	$EuNbO_3 + EuTiO_3$
F	1.04	0.73	3.10	1.00	0.75	3.00	8.11	8.08	$EuNbO_3 + EuTiO_3$
G	0.96	0.76	3.03	1.00	0.81	3.00	7.94	7.76	$EuNbO_3 + EuTiO_3$
H	1.02	0.88	3.07	1.00	0.88	3.00	8.08	8.01	$EuNbO_3 + EuTiO_3$
I	1.01	0.94	3.07	1.00	0.94	3.00	7.99	7.97	$EuNbO_3 + EuTiO_3$
J	1.00	0.94	3.04	1.00	0.95	3.00	8.10	7.94	$EuNbO_3 + EuTiO_3$
K	0.89	0.95	2.93	1.00	0.95	3.00	7.79	7.49	$EuNbO_3 + EuTiO_3$
L	1.00	0.95	3.03	1.00	0.96	3.00	8.08	7.96	$EuNbO_3 + EuTiO_3$
M	0.98	0.96	3.00	1.00	0.96	3.00	8.01	7.84	$EuNbO_3 + EuTiO_3$
N	1.01	0.96	3.07	1.00	0.96	3.00	7.99	7.97	$EuNbO_3 + EuTiO_3$
O	1.02	0.98	3.06	1.00	0.98	3.00	8.02	8.00	$EuNbO_3 + EuTiO_3$
P	1.01	1.00	3.03	1.00	1.00	3.00	8.16	7.96	$EuTiO_3$

a: $\mu_{eff}(calcd.) = \sqrt{x}\mu(Eu^{2+})$, $\mu(Eu^{2+}) = 7.94\ \mu_B$

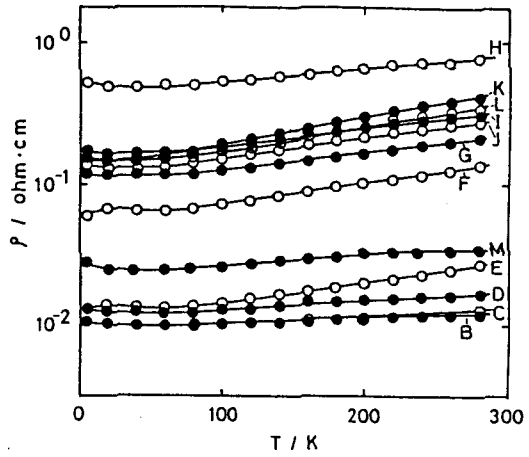

Fig.25. Temperature dependence of electrical resistivities for $[yEuTiO_3 + (1-y)EuNbO_3]$. Symbols in the diagram are experimental numbers in Table 7

are in a bivalent state and that the 4d spins of niobium are paired, since $EuNbO_3$ is a metallic conductor.

Figures 25 and 26 show the temperature dependence of electrical resistivities for the sintered products. The sintered samples with low titanum concentration ($y < 0.96$) are metallic conductors (Fig. 25). However, the sintered products with high titanum concentration ($y > 0.96$) are semiconductors (Fig. 26). The metallic region of sintered $EuTiO_3$ - $EuNbO_3$ is wider than the region of sintered $EuZrO_3$ - $EuNbO_3$.

An activation energy of conduction for semiconductive $EuTiO_3$ - $EuNbO_3$ increased with increasing y. The activation

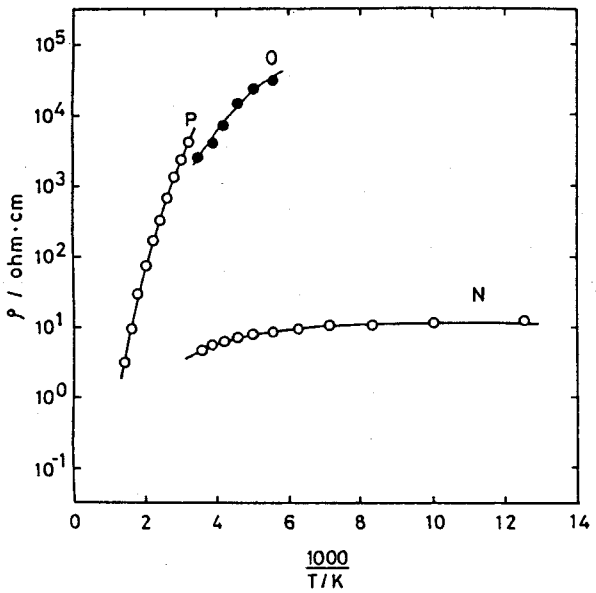

Fig.26. Temperature dependence of electrical resistivities for $[yEuTiO_3 + (1-y)EuNbO_3]$. Symbols in the diagram are experimental numbers in Table 7

energy of conduction for $EuTiO_3$ is 0.48 eV at 800 K, which is considered to be the energy difference between the bottom of conduction band and the $4f^7$ level.

Figure 27 shows the electrical resistivity of the sintered products at 300 K. The resistivity of the samples does not depend on y in the range $0 < y < 0.96$ (the metallic region), and rapidly increases with increasing y at $y \geqq 0.96$ (the semiconductive region).

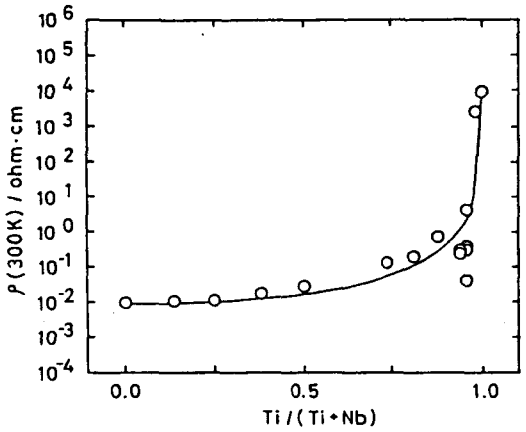

Fig.27. Resistivity at 300 K vs. Ti content for [$yEuTiO_3$ + $(1-y)EuNbO_3$]. Symbols in the diagram are experimental numbers in Table 7

Figure 28 shows the thermal coefficient of resistivity for the sintered products at various y. The thermal coefficient of resistivity varies continuously with y from $+2.8 \times 10^{-3}$ K^{-1} (y = 0.75) to -3.0×10^{-2} K^{-1} (y = 1.0). At y = 0.96, the thermal coefficient is zero.

The electrical resistivity at this composition is 0.1-1.0 ohm·cm, and this value is fairly greater than the resistivity of sintered $EuZrO_3$ - $EuNbO_3$ at Zr/(Zr+Nb) = 0.14. This may be caused by the fact that concentration of $EuNbO_3$ in $EuTiO_3$ - $EuNbO_3$ (y = 0.96) is greater than that in $EuZrO_3$ - $EuNbO_3$ (Zr/(Zr+Nb) = 0.14).

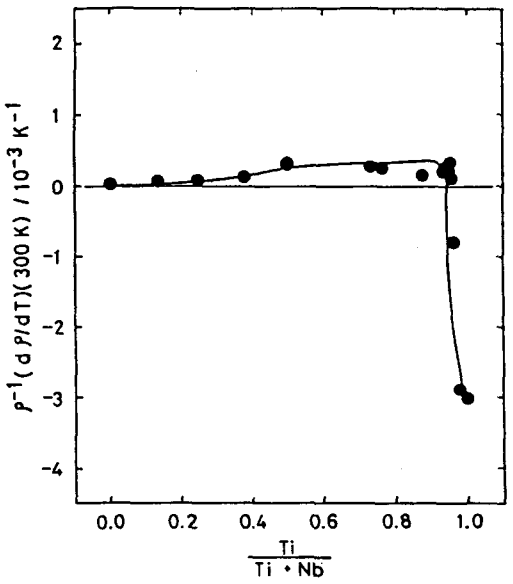

Fig.28. Thermal coefficient of resistivity vs. Ti content for $[yEuTiO_3 + (1-y)EuNbO_3]$

Control of the value of thermal coefficient of resistivity is easier for sintered $EuZrO_3$ - $EuNbO_3$ than for sintered $EuTiO_3$ - $EuNbO_3$, because the region where the former's thermal coefficient of resistivity is near zero is wider than the latter's.

1-4. Summary

Two-phase sintered products $[yEuZrO_3 + (1-y)EuNbO_3]$ and $[yEuTiO_3 + (1-y)EuNbO_3]$ were investigated as electrical resistance materials. The results obtained in this chapter are

as follows.

1. Electrical resistivity of sintered [$yEuZrO_3$ + $(1-y)EuNbO_3$] increased continuously with y, and a transition from a metallic to semiconducting characteristics occured at y = 0.14. The resistivity varied almost linearly with temperature in the range y = 0 to y = 0.24, and thermal coefficients of resistivity at 300 K for the products decreased from $+5.9 \times 10^{-4}$ K^{-1} to -7.4×10^{-4} K^{-1} according to the value of y. At y = 0.14, the thermal coefficient was almost zero.

2. Electrical resistivities of sintered [$yEuTiO_3$ + $(1-y)EuNbO_3$] did not depend on y in the range y = 0-0.96, and rapidly increased with increasing y over y = 0.96. The sintered products were metallic conductors from y = 0 to y = 0.96, and were semiconductors at y > 0.96. Thermal coefficients of resistivity for sintered products varied continuously with y, and became a maximum of 2.8×10^{-3} K^{-1} at y = 0.75 and a minimum around y = 1.00. The coefficient was positive at y < 0.96 and negative at y > 0.96. The absolute value of the thermal coefficient of resistivity minimized, namely $(1/\rho)(d\rho/dT) = 0$, at y = 0.96.

3. Control of the value of thermal coefficient of resistivity was easier for sintered $EuZrO_3$ - $EuNbO_3$ than for sintered $EuTiO_3$ - $EuNbO_3$.

GENERAL CONCLUSION

In this thesis, mixed oxides containing bivalent europium and niobium bave been investigated with respect to syntheses, and their physical and chemical properties. Main results of this work are as follows.

1. Europium (II) niobium bronzes, Eu_xNbO_y (y = 2+x - 3), were prepared by a solid state reaction of Eu_2O_3, Nb_2O_5, and Nb. The oxide Eu_xNbO_3 is in a tetragonal form at x = 0.5-0.65, and in a cubic form at x = 0.65-1.0. Cubic Eu_xNbO_{2+x} is formed at x = 0.5-1.0.
2. Cubic Eu_xNbO_3 and Eu_xNbO_{2+x} exhibit metallic conduction while tetragonal Eu_xNbO_3 is a semiconductor. A band model based on the Goodenough's model was proposed for cubic Eu_xNbO_3 and Eu_xNbO_{2+x} and for tetragonal Eu_xNbO_3.
3. Conduction electrons of cubic Eu_xNbO_3 are almost free and the quasi-free electron model is applicable for the bronze. However, conduction electrons of Eu_xNbO_{2+x} are bound to oxygen vacancies by electrostatic force.
4. Thermal coefficients of the electrical resistivity are very small for cubic europium niobium bronzes, since residual resistivities of these bronzes are large.
5. Two new compound, $Eu_{0.33}Nb_{0.67}O$ and $Eu_{0.5}Nb_{0.5}O$, were found in the system EuO - NbO. The oxide $Eu_{0.33}Nb_{0.67}O$ is a metallic conductor, while $Eu_{0.5}Nb_{0.5}O$ is a semiconductor.
6. Bivalent europium and tetravalent niobium in the bronze are oxidized to Eu^{3+} and Nb^{5+} with atmospheric oxygen. The oxidation

reaction of Eu^{2+} occurs in preference to that of Nb^{4+}. The starting temperature of the oxidation reaction for Eu^{2+} is 550 K for the bronzes.

7. The oxidation mechanism of tetragonal Eu_xNbO_3 differs from that of cubic Eu_xNbO_3. Cubic Eu_xNbO_3 oxidizes to an amorphous phase and the tetragonal one to a complex crystalline phase, and $EuNbO_4$ crystallizes from the amorphous or crystalline phase at 950 K or 1070 K respectively.

8. Electrical properties of sintered $EuZrO_3$ - $EuNbO_3$ and $EuTiO_3$ - $EuNbO_3$ have been investigated so as to develop a new electrical resistor material. Sintered $EuZrO_3$ - $EuNbO_3$ is excellent for the resistor material, because thermal coefficient of electrical resistivity is almost zero at Zr/(Zr+Nb) = 0.96.

ACKNOWLEDGEMENT

The author is greatly indebted to Professor Jiro Shiokawa of Faculty of Engineering, Osaka University for his continuing guidance and encouragement throughout this work.

The author is also indebted to Professor Hideo Tamura and Professor Toshio Tanaka for their kind suggestions in the course of this thesis.

The author is very grateful to Associate Professor Gin-ya Adachi for his significant direction during this work, and for his kind suggestions in the preparation of the manuscripts.

The author would like to acknowledge Mr. Yoshiyuki Hirashima, Dr. Tsuyoshi Arakawa, Dr. Tsutomu Shin-ike and Mrs. Ichiko Kawamoto for their significant discussion.

Thanks are given to the author's co-workers, Dr. Kazunao Sato, Mr. Masatake Hasegawa, and Miss Midori Tanida for their assistance, and Dr. Mineo Sato, Dr. Tetuo Sakai, Dr. Ken-ichi Machida, Mr. Kunihiko Mizumoto, and all the other members of Shiokawa laboratory for their help and valuable suggestions.

Finally, the author wished to express his gratitude to his parents from the bottom of his heart for their encouragement and understanding on this work.

REFERENCES

1. K. A. Gschneidner, Jr., "Rare Earth Alloys", University Microfirms, Xerox Company, Ann Arbor, Michigan, U.S.A., 1973.
2. H. D. Edward, "Electrochemical and Spectroscopic Studies of Some Less Stable Oxidation States of Selected Lanthanide and Actinide Elements", University Microfilms International, Ann Arbor, Michigan, U.S.A., 1982.
3. K. W. Bagnall, "Lanthanides and Actinides", Inorganic Chemistry, Series I, Vol. 7, K. W. Bagnall, Ed., University Park Press, Baltimore, MD, 1972.
4. D. T. Sawyer and J. L. Roberts, Jr., "Experimental Electrochemistry for Chemists", John Wiley and Sons, New York, NY, 1974.
5. L. J. Nugent, R. D. Baybarz, J. L. Burnett, and J. L. Ryan, J. Phys. Chem., 77, 1528 (1973).
6. W. T. Carnall, in "Handbook on the Physics and Chemistry of Rare Earths", K. A. Gschneidner, Jr. and L. Eyring, Eds., North-Holland, Amsterdam, 1979, Vol. 3, Chap. 24.
7. M. W. Shafer, T. R. McGuire, and J. C. Suits, Phys. Rev. Lett., 11, 251 (1963).
8. J. Brous, I. Fankuchen, and E. Banks, Acta Crystallogr., 6, 67 (1953).
9. M. W. Shafer, J. Appl. Phys., 36, 1145 (1965).
10. G. J. McCarthy, W. B. White, and R. Roy, J. Inorg. Nucl. Chem., 31, 329 (1969).
11. J. E. Greedan and G. J. McCarthy, Mat.Res. Bull., 7, 531

(1972).

12. H. Holzapfel and J. Sieler, Z. Anorg. Allg. Chem., 343, 174 (1966).

13. T. R. McGuire, M. W. Schafer, R. J. Joenk, H. A. Alperin, and S. T. Pickart, J. Appl. Phys., 37, 981 (1966).

14. A. M. Lejus, C. R. Acad. Sci., Ser. C, 272, 462 (1971).

15. J. Sieler and J. Kaiser, Z. Anorg. Allg. Chem., 377, 316 (1970).

16. C. L. Chien and J. Kaiser, Z. Anorg. Allg. Chem., 377, 316 (1970).

17. C. L. Chien and F. de S. Barros, Phys. Lett. A, 38, 427 (1972).

18. C. DeLamarre, Rev. Int. Hautes Temp. Refract., 9, 209 (1972).

19. G. Desgardin, J. P. Fayolle, and B. Raveau, C. R. Acad. Sci., Ser. C, 276, 1101 (1973).

20. G. J. McCarthy and J. E. Greedan, Inorg. Chem., 14, 772 (1975).

21. J. E. Greedan, G. J. McCarthy, and C. Sipe, Inorg. Chem., 14, 775 (1975).

22. D. Ridgley and R. Ward, J. Am. Chem. Soc., 77, 6132 (1955).

23. J. B. Goodenough, in "Progress in Solid State Chemistry", Vol. V, H. Reiss, Ed., Pergamon Press, Inc., Oxford and New York (1972).

24. J. B. Goodenough, J. Appl. Phys., 37, 1415 (1966).

25. G. Hägg, Z. Phys. Chem., 29,192 (1935).

26. Z. I. Ornatskaya, Zh. Tekh. Fiz., 27, 130 (1957).

27. H. Wright, Ann. Chem. Pharm., 79, 223 (1951).

28. M. E. Straumanis and A. Dravhieks, J. Am. Chem. Soc., 71, 683 (1949).

29. E. J. Huibregste, D. B. Barker, and C. C. Danielson, Phys. Rev., 84, 142 (1951).

30. B. W. Brown and E. Banks, Phys. Rev., 84, 609 (1951).

31. W. R. Gardner and G. C. Danielson, Phys. Rev., 93, 46 (1954).

32. L. D. Ellerbeck, H. R. Shanks, P. H. Sidles, and G. C. Danielson, J. Chem. Phys., 35, 298 (1961).

33. L. P. Muhlestein and G. C. Danielson, Phys. Rev., 158, 158 (1967).

34. L. P. Muhlestein and G. C. Danielson, Phys. Rev., 160, 562 (1967).

35. R. Fuchs, J. Chem. Phys., 42, 3781 (1965).

36. J. B. Goodenough, Bull. Soc. Chim. France, 4, 1200 (1965).

37. R. D. Schannon, Acta Crystogr., Sect. A, 32, 751 (1976).

38. J. P. Fayolle, F. Studer, G. Desgurdin, and B. Raveau, J. Solid State Chem., 13, 57 (1975).

39. F. Studer and B. Raveau, Acta Crystogr., Sect. B, 31, 2774 (1975).

40. G. V. Bazuev, O. V. Makarova, and G. P. Shveikin, Dokl. Akad. Nauk SSSR, 223, 358 (1975).

41. K. Ridgley and R. J. Ward, J. Am. Chem. Soc., 77, 6132 (1955).

42. F. Studer, J. P. Fayolle, and B. Raveau, Mat. Res. Bull., 11, 1125 (1976).

43. F. Studer, G. Allais, and B. Raveau, J. Phys. Chem. Solids, 41, 1187 (1980).

44. F. Studer, G. Allais, and B. Raveau, J. Phys. Chem. Solids, 41, 1199 (1980).

45. N. N. Greenwood, F. Viegas, and F. Studer, J. Solid State Chem., 31, 347 (1980).

46. N. Cusack and P. Kendall, Proc. Phys. Soc., 72, 898 (1958).

47. E. I. Krylov, E. M. Elovskikh, G. G. Kasimov, and B. D. Filin, Zh. Obshch. Khim., 44, 1836 (1974).

48. J. B. Goodenough and J. A. Kafalas, J. Solid State Chem., 6, 493 (1973).

49. B. L. Crowder and M. J. Sienko, J. Chem. Phys., 38, 1576 (1963).

50. M. Atoji and R. E. Rundle, J. Chem. Phys., 32, 627 (1960).

51. B. W. Brown and E. Banks, J. Am. Chem. Soc., 76, 963 (1954).

52. J. Bardeen and W. Shockley, Phys. Rev., 80, 72 (1952).

53. E. H. Greener, D. H. Whithmore, and M. E. Fine, J. Chem. Phys., 34, 1017 (1960).

54. D. J. Howarth and E. H. Sondheimer, Proc. R. Soc. London, Ser. A, 219, 53 (1953).

55. D. R. Kundrak and M. J. Sienko, Inorg. Chem., 6, 880 (1967).

56. M. R. Oliver, J. O. Dimmock, and T. B. Reed, IBM. J. Res. Dev., 14, 276 (1970).

57. Y. Shapira, S. Foner, and T. B. Reed, Phys. Rev. B, 8, 2299. (1973).

58. Y. Shapira, S. Foner, R. Aggarwal, and T. B. Reed, Phys. Rev. B, 8, 2316 (1973).

59. J. Birecki, H. E. Stanley, and Y. Shapira, Phys. Rev. B, 8, 2327 (1973).

60. P. G. de Gennes and J. Friedel, J. Phys. Chem. Solids, 4,

71 (1958).

61. D. J. Kim, Prog. Theor. Phys., 31, 921 (1964).

62. M. E. Fisher and J. S. Langer, Phys. Rev. Lett., 20, 665 (1968).

63. "CRC Handbook of Chemistry and Physics", The Chemical Rubber, C.O., Cleveland, Ohio (1970-1971), p. D45.

64. H. Holzapfel and J. Sieler, Z. Anorg. Allg. Chem., 377, 316 (1970).

65. R. F. Janninck and D. H. Whitmore, J. Phys. Chem. Solids, 27, 1183 (1966).

66. G. G. Kasimov, E. M. Elovskikh, B. P. Filin, and V. G. Teplov, Zh. Obshch. Khim., 45, 1390 (1975).